2025 ML4LM Webinar Series

EarthMind S2S: A coupled ocean-atmosphere-land global AI model for subseasonal to seasonal forecasts

Manmeet Singh
manmeet.singh@utexas.edu

GLASS GEWEX / Land - Atmosphere System Studies

WKU

Machine Learning 4 Land Surface Model

REVIEW

doi:10.1038/nature14956

The quiet revolution of numerical weather prediction

Peter Bauer[1], Alan Thorpe[1] & Gilbert Brunet[2]

Advances in numerical weather prediction represent a quiet revolution because they have resulted from a steady accumulation of scientific knowledge and technological advances over many years that, with only a few exceptions, have not been associated with the aura of fundamental physics breakthroughs. Nonetheless, the impact of numerical weather prediction is among the greatest of any area of physical science. As a computational problem, global weather prediction is comparable to the simulation of the human brain and of the evolution of the early Universe, and it is performed every day at major operational centres across the world.

At the turn of the twentieth century, Abbe[1] and Bjerknes[2] proposed that the laws of physics could be used to forecast the weather; they recognized that predicting the state of the atmosphere could be treated as an initial value problem of mathematical physics, wherein future weather is determined by integrating the governing partial differential equations, starting from the observed current weather. This proposition, even with the most optimistic interpretation of Newtonian determinism, is all the more audacious given that, at that time, there were few routine observations of the state of the atmosphere, no computers, and little understanding of whether the weather possesses any significant degree of predictability. But today, more than 100 years later, this paradigm translates into solving daily a system of nonlinear

use of observational information from satellite data providing global coverage.

More visible to society, however, are extreme events. The unusual path and intensification of hurricane Sandy in October 2012 was predicted 8 days ahead, the 2010 Russian heat-wave and the 2013 US cold spell were forecast with 1–2 weeks lead time, and tropical sea surface temperature variability following the El Niño/Southern Oscillation phenomenon can be predicted 3–4 months ahead. Weather and climate prediction skill are intimately linked, because accurate climate prediction needs a good representation of weather phenomena and their statistics, as the underlying physical laws apply to all prediction time ranges. This Review explains the fundamental scientific basis of numerical

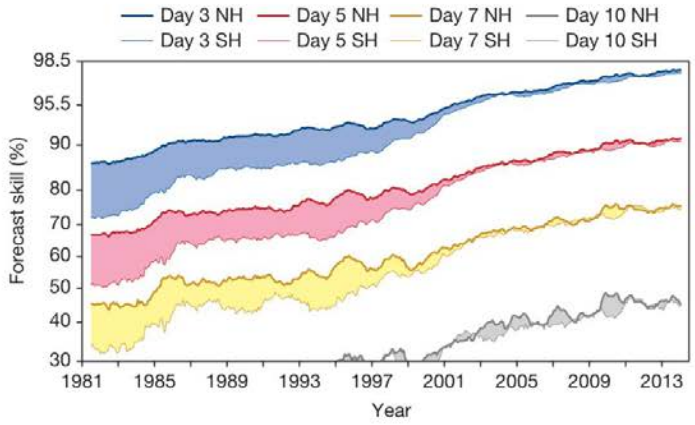

Figure 1 | A measure of forecast skill at three-, five-, seven- and ten-day ranges, computed over the extra-tropical northern and southern hemispheres. Forecast skill is the correlation between the forecasts and the verifying analysis of the height of the 500-hPa level, expressed as the anomaly with respect to the climatological height. Values greater than 60% indicate useful forecasts, while those greater than 80% represent a high degree of accuracy. The convergence of the curves for Northern Hemisphere (NH) and Southern Hemisphere (SH) after 1999 indicates the breakthrough in exploiting satellite data through the use of variational data[100].

Bauer, P., Thorpe, A. and Brunet, G., 2015. The quiet revolution of numerical weather prediction. *Nature*, *525*(7567), pp.47-55.

Deep Learning for Weather Prediction (DLWP)

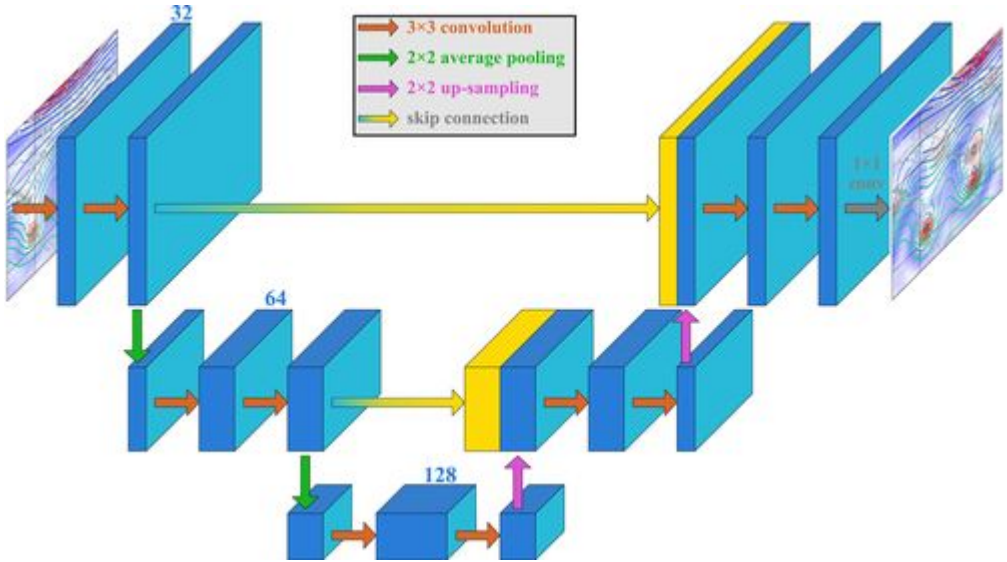

Weyn, J.A., Durran, D.R. and Caruana, R., 2019. Can machines learn to predict weather? Using deep learning to predict gridded 500-hPa geopotential height from historical weather data. *Journal of Advances in Modeling Earth Systems*, *11*(8), pp.2680-2693.

DLWP Cubed Sphere

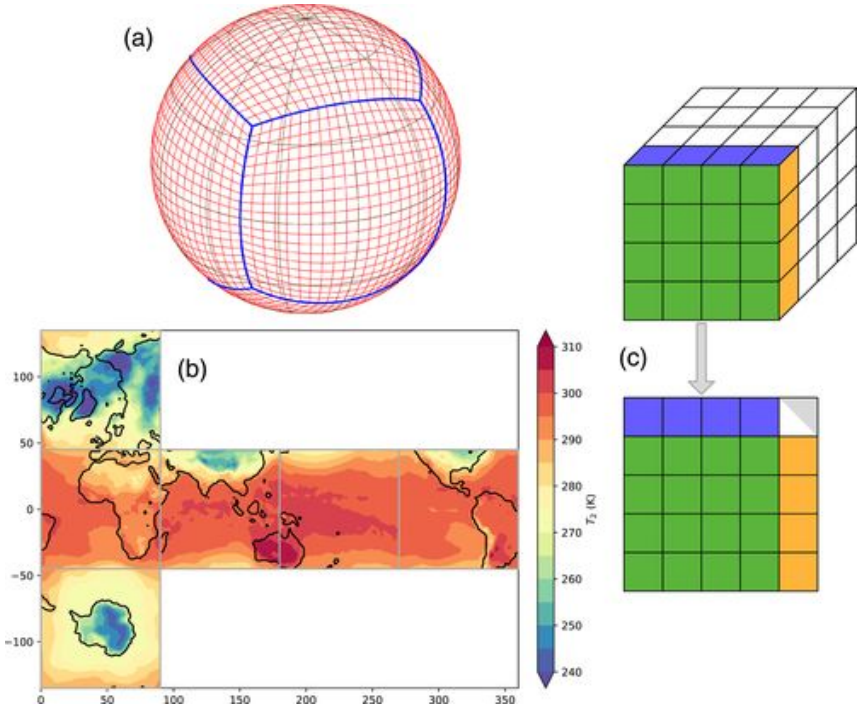

Weyn, J.A., Durran, D.R. and Caruana, R., 2020. Improving data-driven global weather prediction using deep convolutional neural networks on a cubed sphere. Journal of Advances in Modeling Earth Systems, 12(9), p.e2020MS002109.

Deep learning for global precipitation prediction

- DLWP and DLWP-CS use temperature at 850 hPa and geopotential at 500 hPa to show comparable and improved performance w.r.t operational models.
- DLWP and DLWP-CS use global domain for data-driven weather forecasting.
- Previous studies either use **limited regions**, do not consider **spherical distortion**, use fields **simpler** to simulate relative to precipitation, do not compare with **operational forecasts** or do not use **CNN**s limiting their capability to capture spatial patterns.
- Need for a system dedicated to global precipitation forecasts which can be considered a digital twin of the real system.

Modified DLWP-CS

Transforms DLWP-CS from a temporal mapping to a function simulating precipitation from different fields

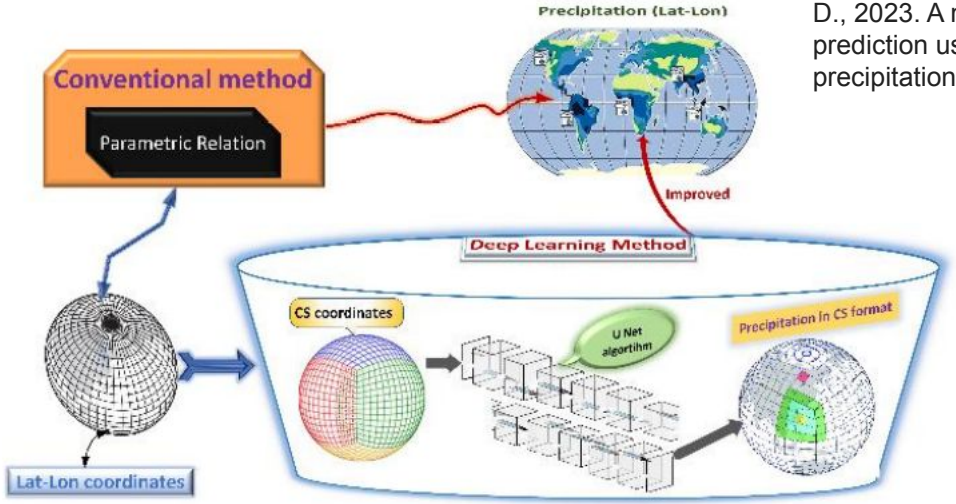

Singh, M., Acharya, N., Patel, P., Jamshidi, S., Yang, Z.L., Kumar, B., Rao, S., Gill, S.S., Chattopadhyay, R., Nanjundiah, R.S. and Niyogi, D., 2023. A modified deep learning weather prediction using cubed sphere for global precipitation. *Frontiers in Climate*, *4*, p.1022624.

WeatherBench

Weatherbench dataset corresponding to total cloud cover and two meter air temperature as precursors and precipitation as the label/target. Training: 1979-2009, Validation: 2010-2011, Testing: 2012-2015. Temporal resolution: hourly

Total Cloud Cover

Surface air temperature

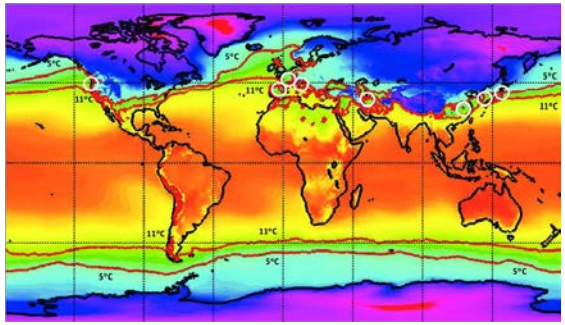

Precipitation

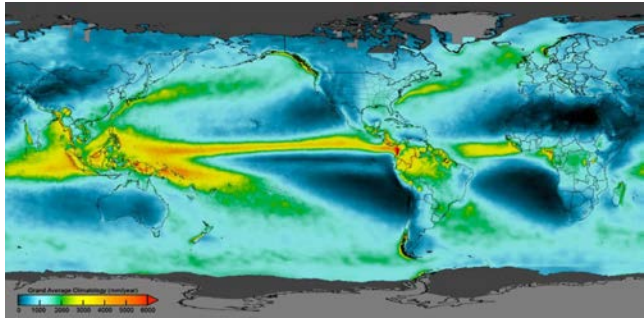

Rasp, S., Dueben, P.D., Scher, S., Weyn, J.A., Mouatadid, S. and Thuerey, N., 2020. WeatherBench: a benchmark data set for data-driven weather forecasting. Journal of Advances in Modeling Earth Systems, 12(11), p.e2020MS002203.

Median of Day-1 precipitation

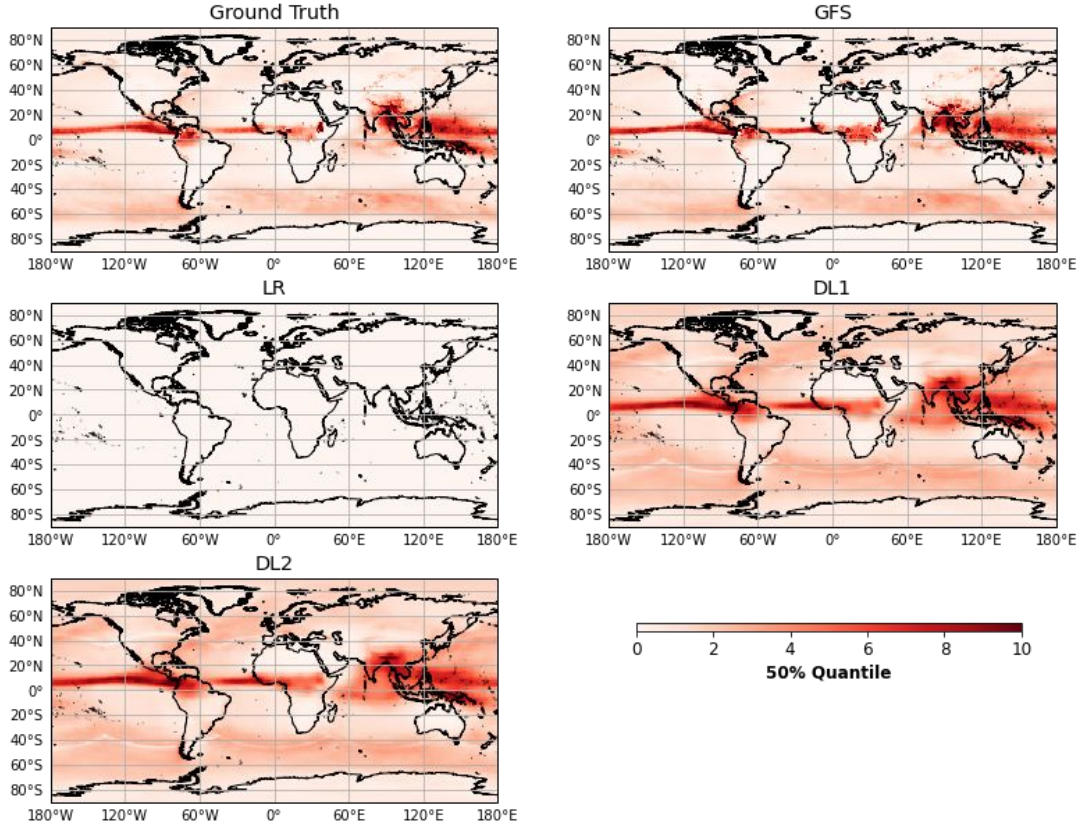

Singh, M., Acharya, N., Patel, P., Jamshidi, S., Yang, Z.L., Kumar, B., Rao, S., Gill, S.S., Chattopadhyay, R., Nanjundiah, R.S. and Niyogi, D., 2023. A modified deep learning weather prediction using cubed sphere for global precipitation. *Frontiers in Climate*, *4*, p.1022624.

Grid point correlations for 2012-2015

- DL1- Total cloud cover as input, DL2 - Surface air temperature as input
- Grid point correlations show that DL1 and DL2 outperform GFS and linear regression
- Comparability to GFS at 24 hour lead assuming that the input fields to precipitation parameterization do not significantly deviate from the observed states

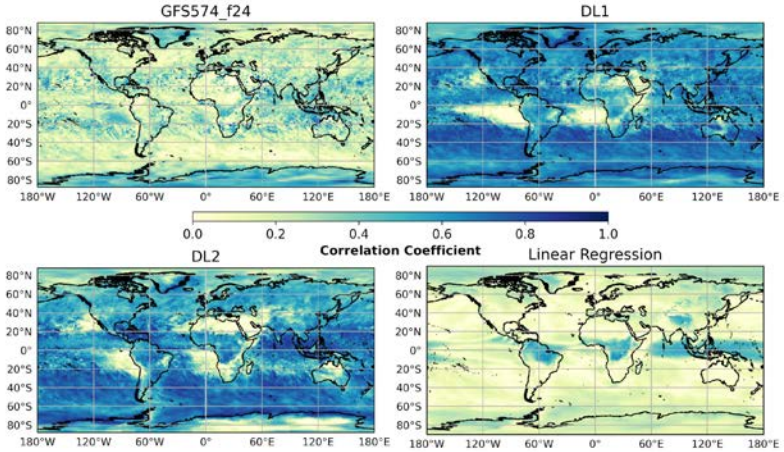

Singh, M., Acharya, N., Patel, P., Jamshidi, S., Yang, Z.L., Kumar, B., Rao, S., Gill, S.S., Chattopadhyay, R., Nanjundiah, R.S. and Niyogi, D., 2023. A modified deep learning weather prediction using cubed sphere for global precipitation. *Frontiers in Climate*, *4*, p.1022624.

Evaluation of modified DLWP-CS

Region	GFS (baseline)	MDLWP-CS
Canada (50-70N, 130-90W)	0.74	0.82
North Asia (50-70N, 25-140E)	0.80	0.70
Europe (44-54N, 40-100E)	0.79	0.86
United States (32-50N, 110-80W)	0.75	0.84
Central Asia (35-50N, 40-100E)	0.79	0.65
Amazon (5N-10S, 50-70W)	0.69	0.88
Equatorial Africa (10N-10S, 14-35E)	0.64	0.76
South Asia (18-35N, 70-90E)	0.90	0.94

Index of agreement for the precipitation averaged over different land regions from (a) GFS and (b) MDLWP-CS models with ERA5 precipitation for the test years 2012–2015.

Singh, M., Acharya, N., Patel, P., Jamshidi, S., Yang, Z.L., Kumar, B., Rao, S., Gill, S.S., Chattopadhyay, R., Nanjundiah, R.S. and Niyogi, D., 2023. A modified deep learning weather prediction using cubed sphere for global precipitation. *Frontiers in Climate*, *4*, p.1022624.

Short-range forecasts of global precipitation using deep learning-augmented numerical weather prediction

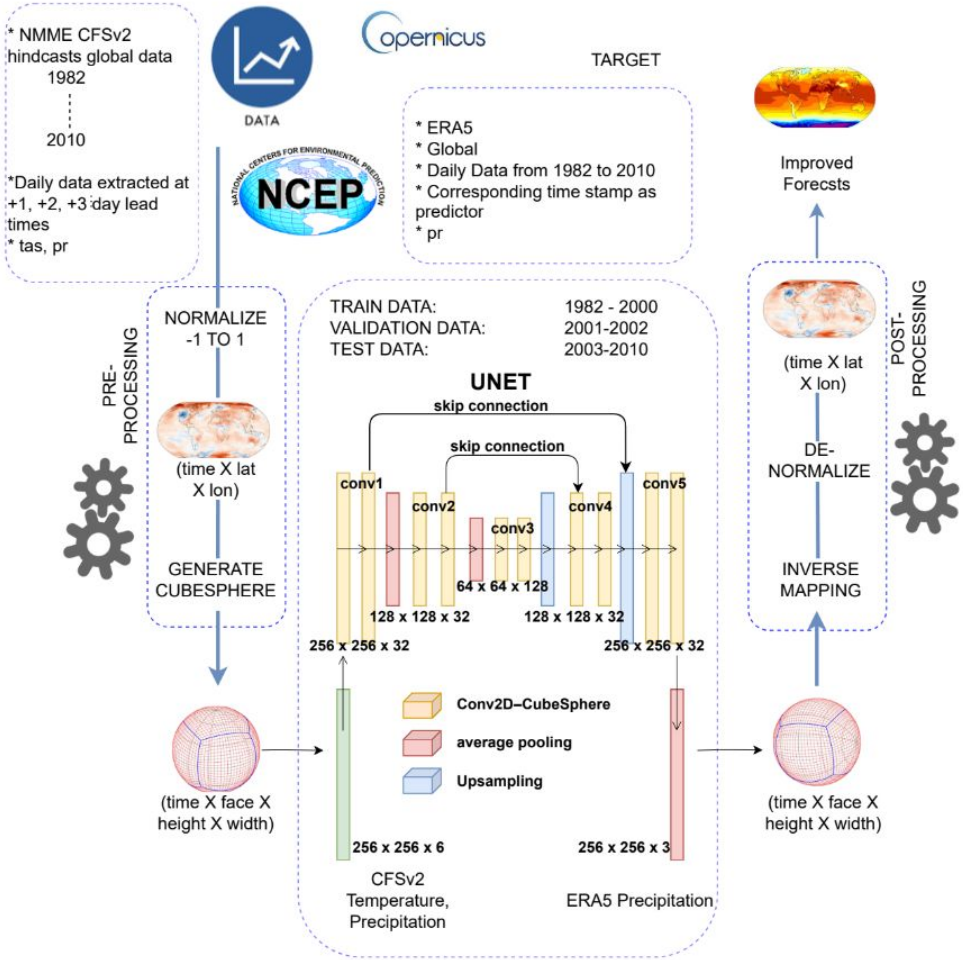

Figure 1: Schematic of the deep learning-augmented numerical weather prediction.

Singh, M., Acharya, N., Grover, A., Rao, S.A., Kumar, B., Yang, Z.L. and Niyogi, D., Short-range forecasts of global precipitation using deep learning-augmented numerical weather prediction. *NeurIPS 2022*

Baseline

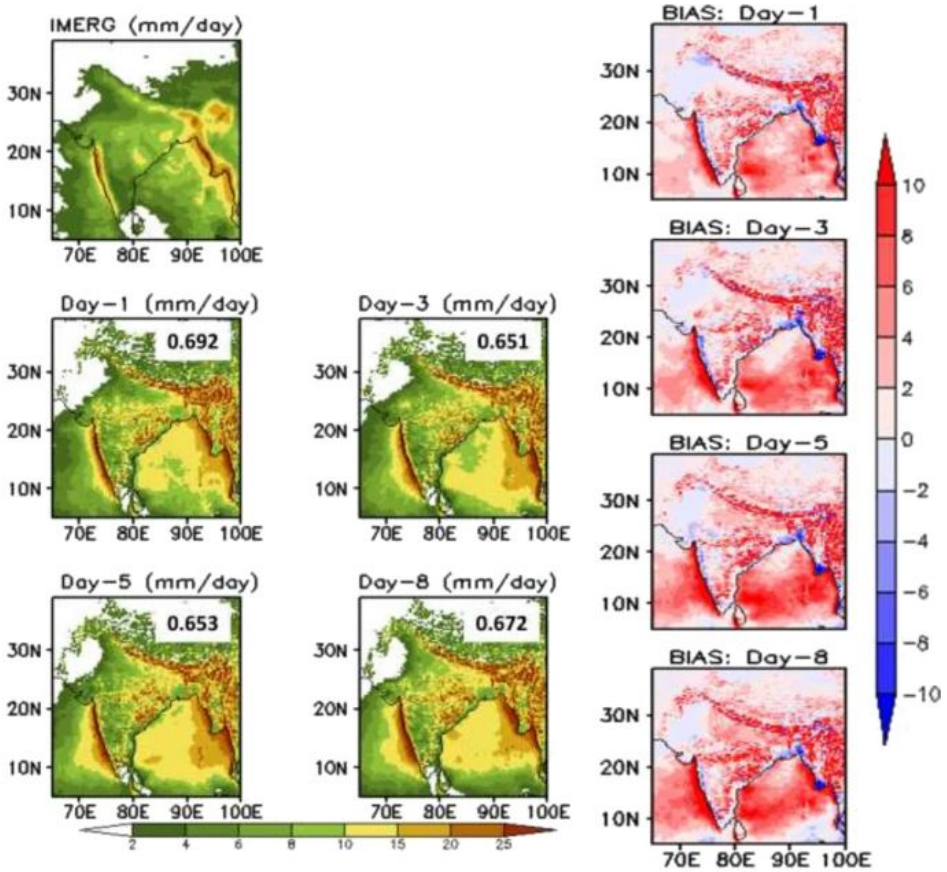

P Mukhopadhyay, VS Prasad, R Krishna, Medha Deshpande, Malay Ganai, Snehlata Tirkey, Sahadat Sarkar, Tanmoy Goswami, CJ Johny, Kumar Roy, et al. Performance of a very high-resolution global forecast system model (gfs t1534) at 12.5 km over the indian region during the 2016–2017 monsoon seasons. Journal of Earth System Science, 128(6):1–18, 2019

Average bias in rainfall (JJA)

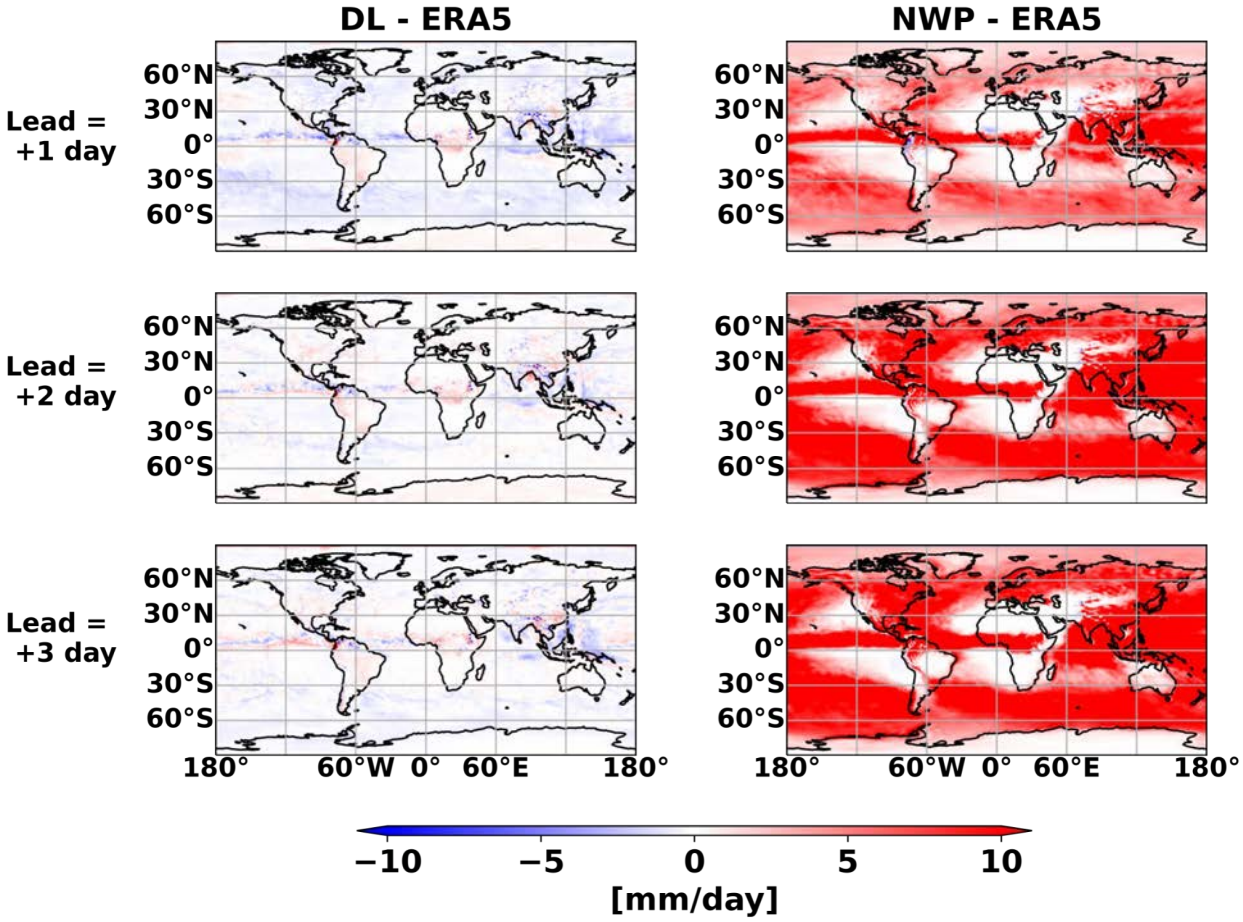

Singh, M., Acharya, N., Grover, A., Rao, S.A., Kumar, B., Yang, Z.L. and Niyogi, D., Short-range forecasts of global precipitation using deep learning-augmented numerical weather prediction. *NeurIPS 2022*

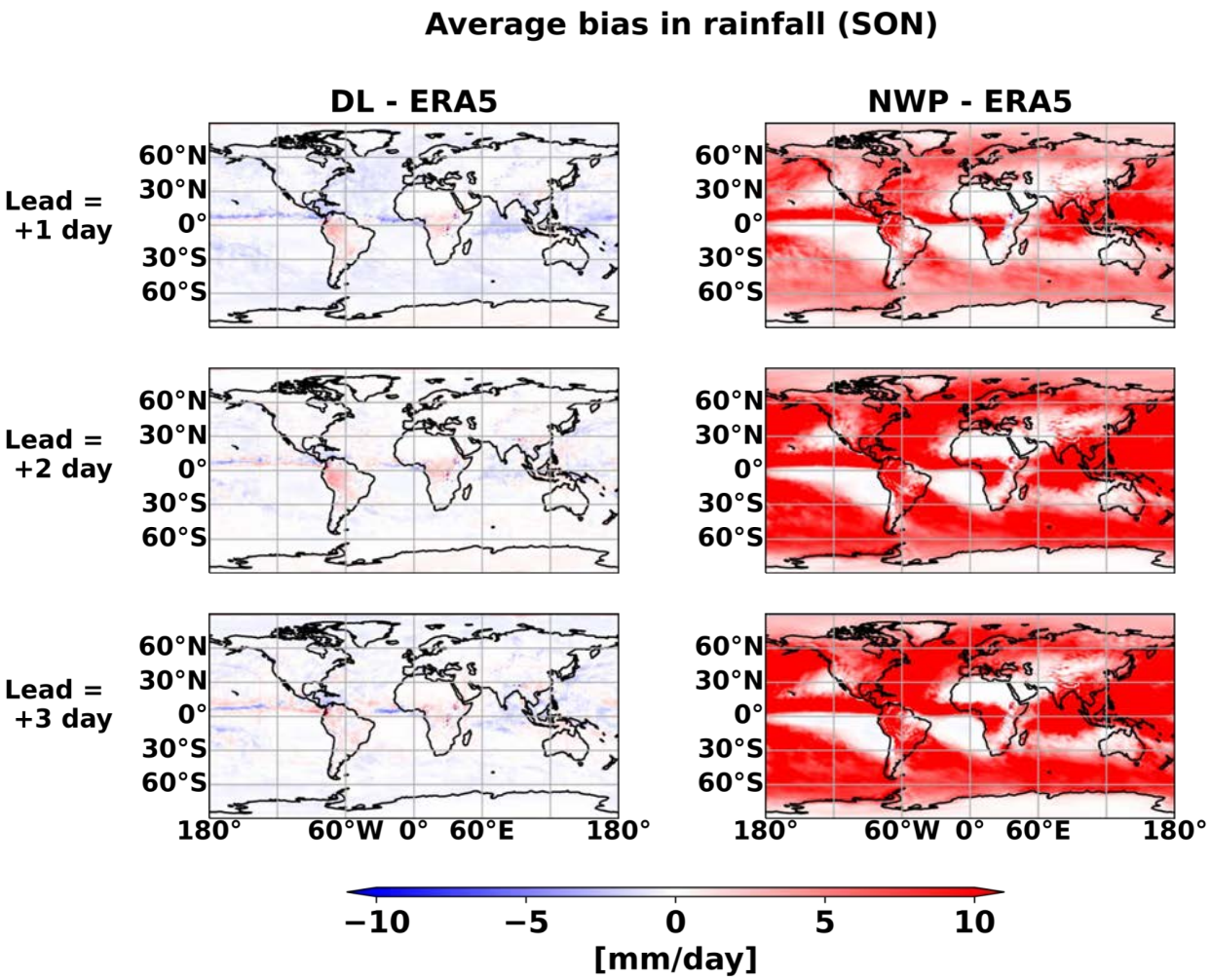

Singh, M., Acharya, N., Grover, A., Rao, S.A., Kumar, B., Yang, Z.L. and Niyogi, D., Short-range forecasts of global precipitation using deep learning-augmented numerical weather prediction. *NeurIPS 2022*

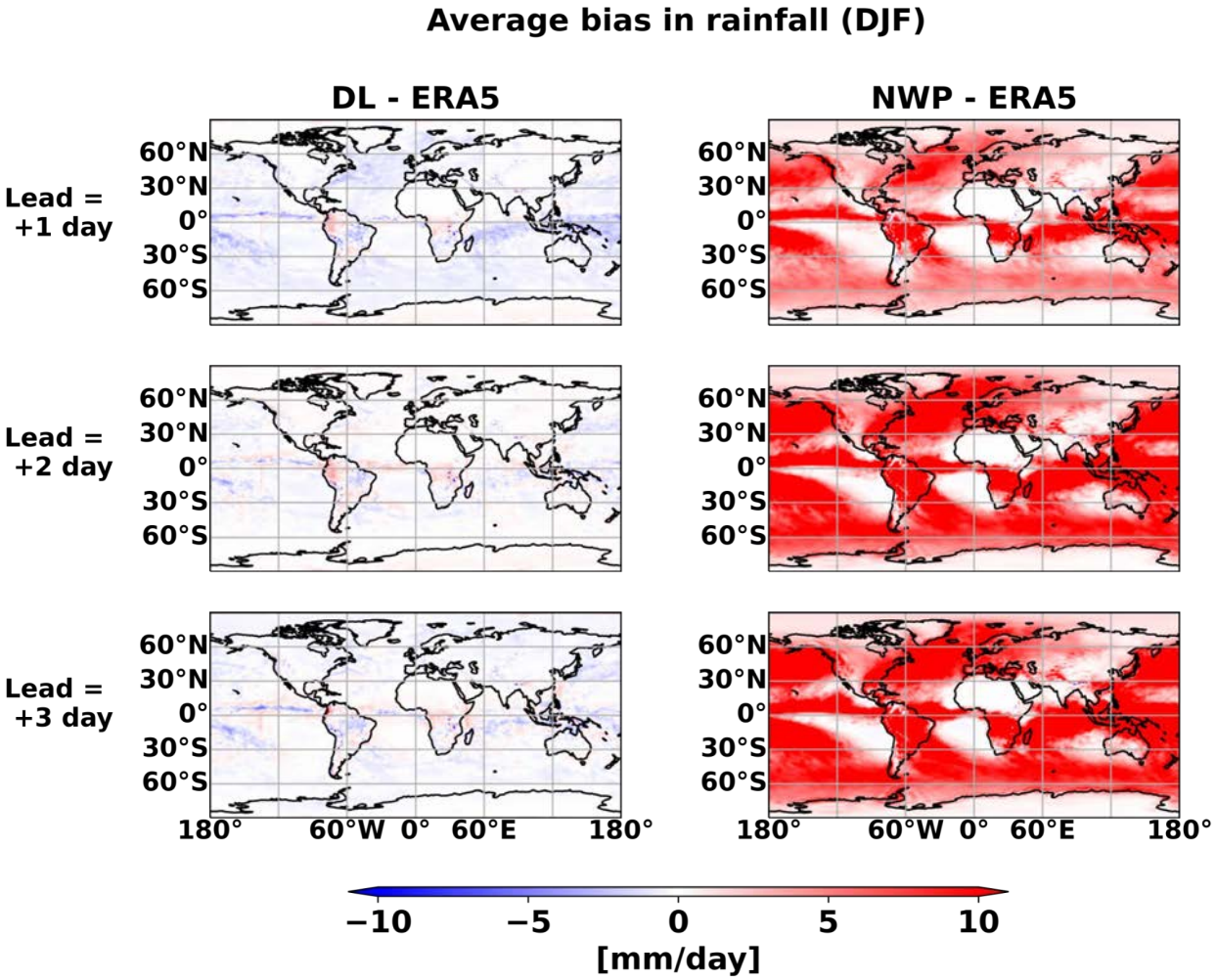

Singh, M., Acharya, N., Grover, A., Rao, S.A., Kumar, B., Yang, Z.L. and Niyogi, D., Short-range forecasts of global precipitation using deep learning-augmented numerical weather prediction. *NeurIPS 2022*

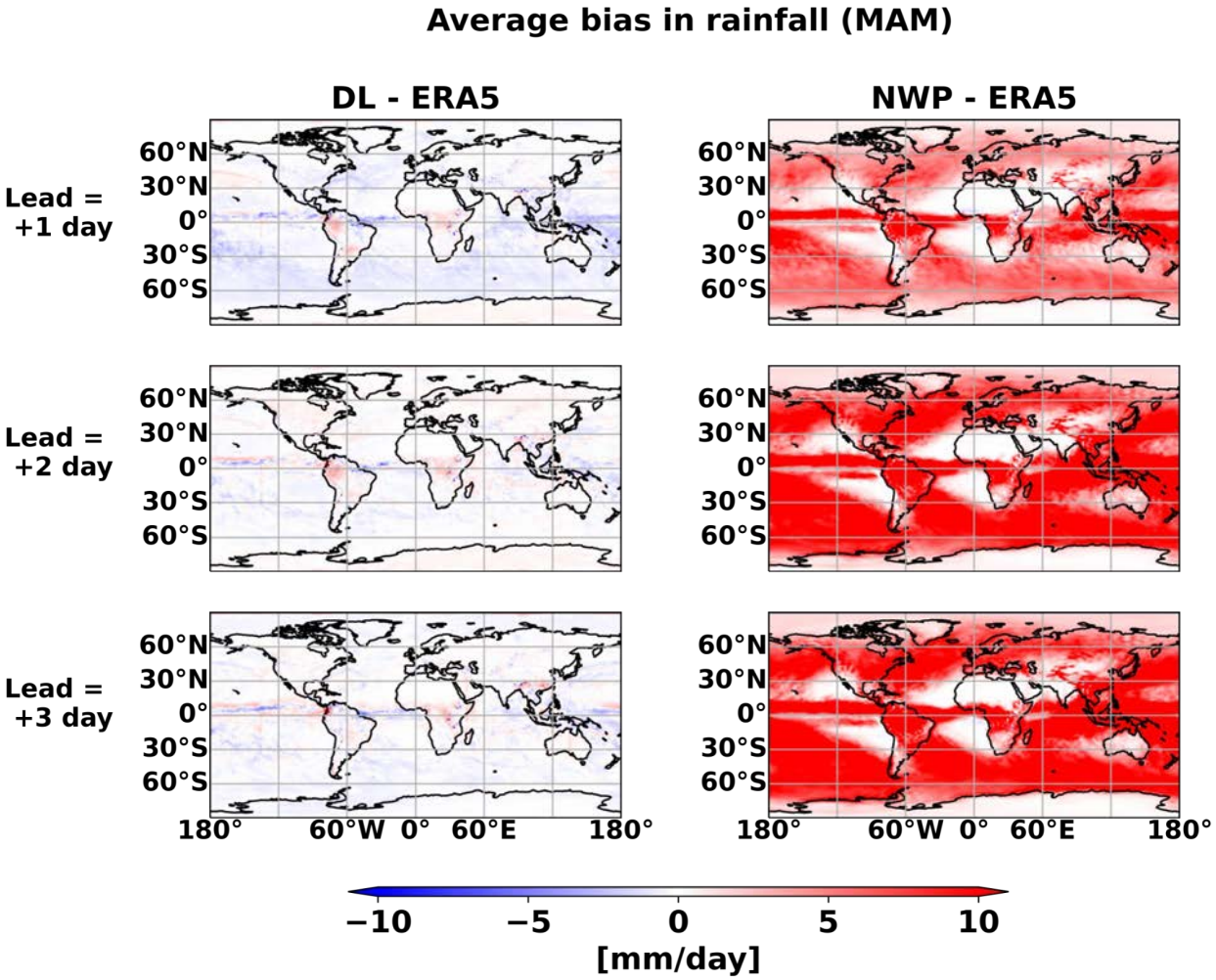

Singh, M., Acharya, N., Grover, A., Rao, S.A., Kumar, B., Yang, Z.L. and Niyogi, D., Short-range forecasts of global precipitation using deep learning-augmented numerical weather prediction. *NeurIPS 2022*

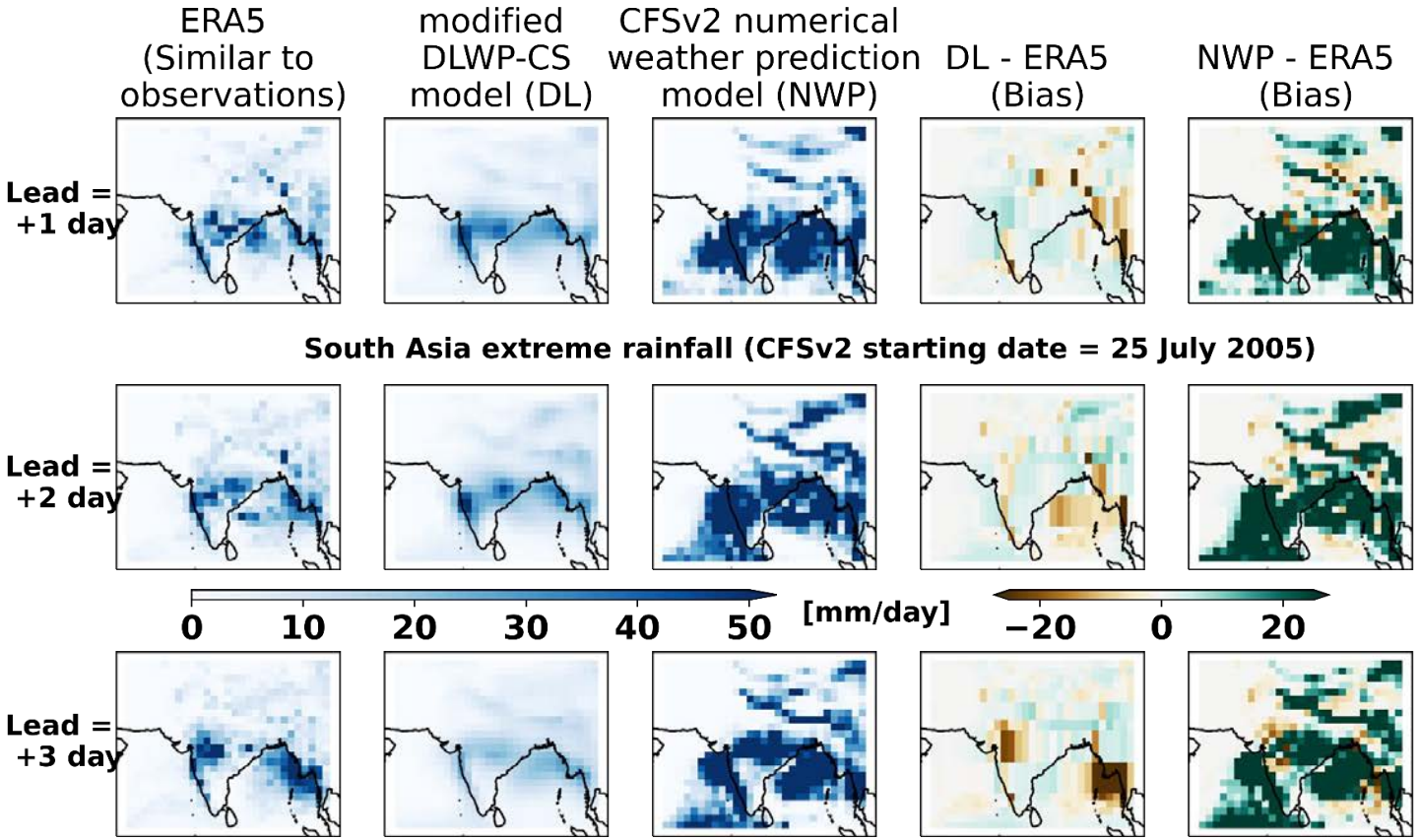

Singh, M., Acharya, N., Grover, A., Rao, S.A., Kumar, B., Yang, Z.L. and Niyogi, D., Short-range forecasts of global precipitation using deep learning-augmented numerical weather prediction. *NeurIPS 2022*

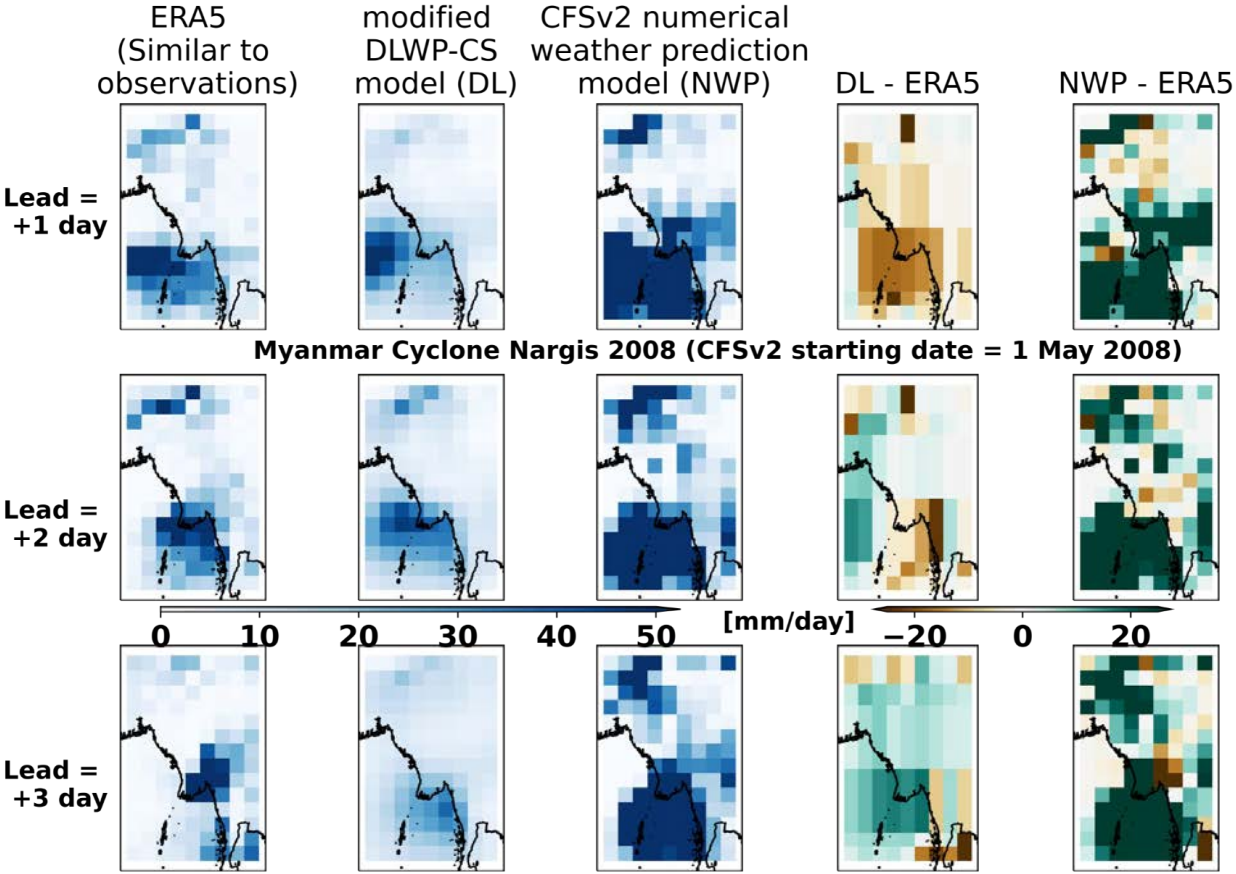

Singh, M., Acharya, N., Grover, A., Rao, S.A., Kumar, B., Yang, Z.L. and Niyogi, D., Short-range forecasts of global precipitation using deep learning-augmented numerical weather prediction. *NeurIPS 2022*

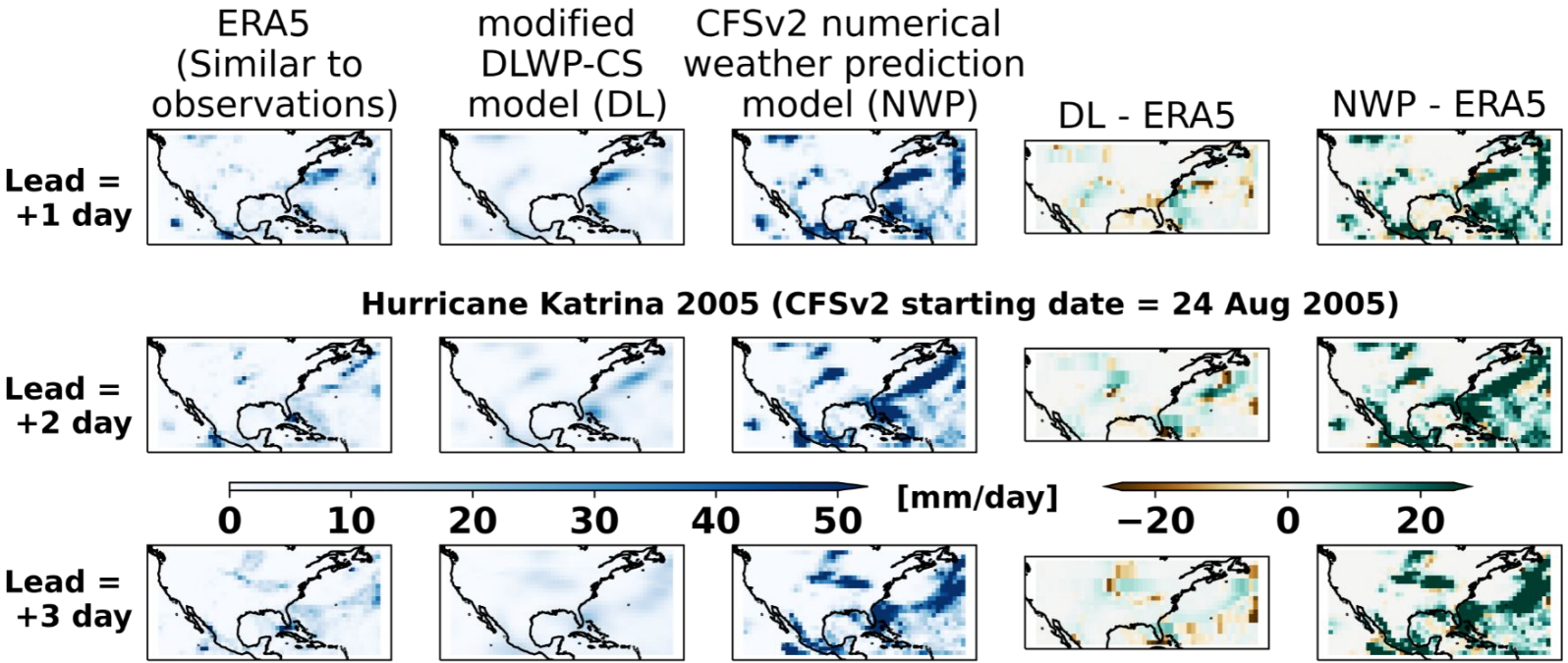

Singh, M., Acharya, N., Grover, A., Rao, S.A., Kumar, B., Yang, Z.L. and Niyogi, D., Short-range forecasts of global precipitation using deep learning-augmented numerical weather prediction. *NeurIPS 2022*

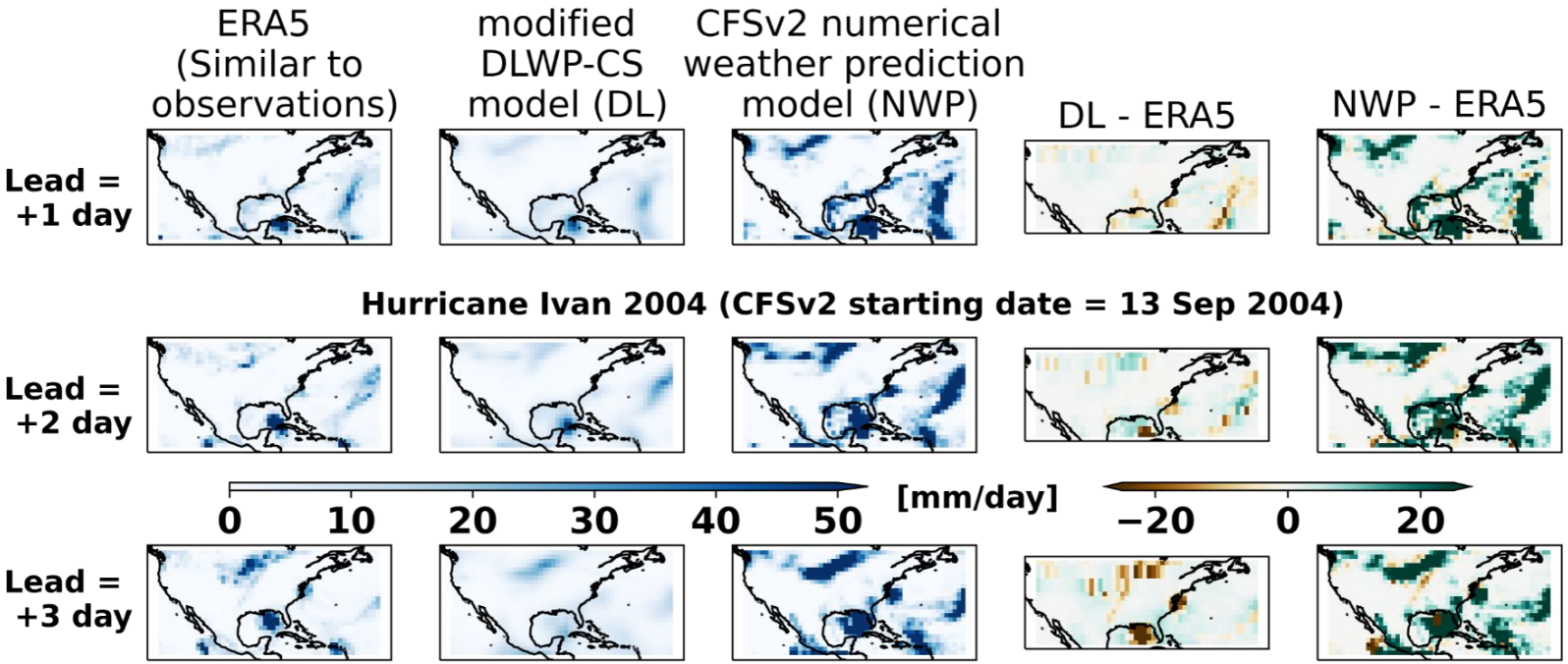

Singh, M., Acharya, N., Grover, A., Rao, S.A., Kumar, B., Yang, Z.L. and Niyogi, D., Short-range forecasts of global precipitation using deep learning-augmented numerical weather prediction. *NeurIPS 2022*

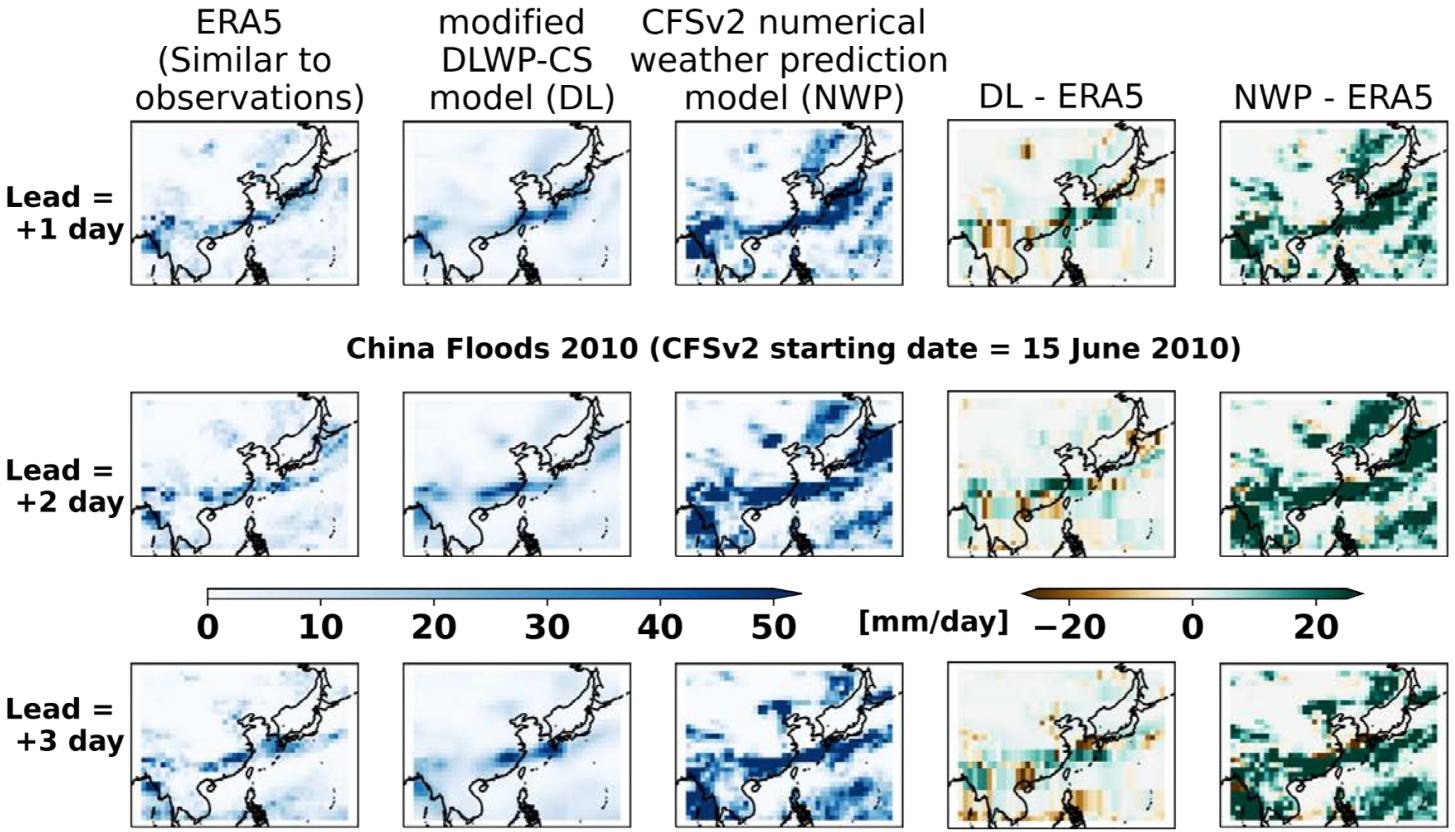

Singh, M., Acharya, N., Grover, A., Rao, S.A., Kumar, B., Yang, Z.L. and Niyogi, D., Short-range forecasts of global precipitation using deep learning-augmented numerical weather prediction. *NeurIPS 2022*

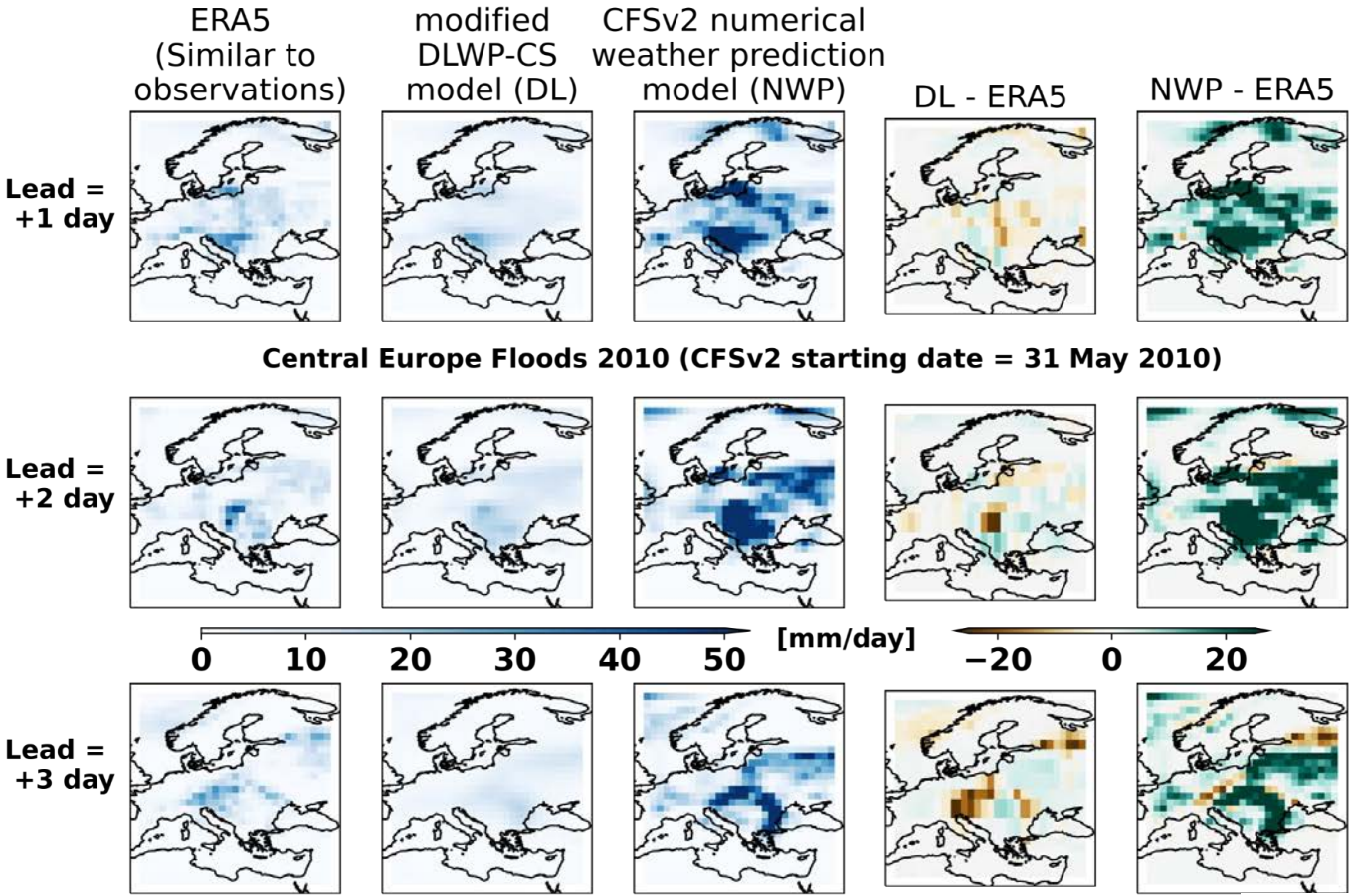

Singh, M., Acharya, N., Grover, A., Rao, S.A., Kumar, B., Yang, Z.L. and Niyogi, D., Short-range forecasts of global precipitation using deep learning-augmented numerical weather prediction. *NeurIPS 2022*

Season	Lead = 1 day (mm/day)		Lead = 2 day (mm/day)		Lead = 3 day (mm/day)	
	DL - ERA5	CFSv2 - ERA5	DL - ERA5	CFSv2 - ERA5	DL - ERA5	CFSv2 - ERA5
DJF	**-0.3**	3.827	**0.022**	7.66	**-0.158**	7.657
MAM	**-0.282**	3.834	**0.032**	7.811	**-0.11**	7.89
JJA	**-0.334**	3.97	**-0.02**	8.102	**-0.115**	8.239
SON	**-0.299**	3.954	**0**	7.95	**-0.148**	7.972

Table 1. Performance of the deep learning augmented numerical weather prediction system CFSv2 versus CFSv2 alone. The table shows global average bias/error in simulating precipitation by the hybrid deep learning and CFSv2 system versus CFSv2 alone. DJF (December to February), MAM (March to May), JJA (June to August) and SON (September to November) represent the different months of an year. The performance is shown for the entire test period from the year 2003 to 2010

Events	Lead = 1 day (mm/day)		Lead = 2 day (mm/day)		Lead = 3 day (mm/day)	
	DL - ERA5	CFSv2 - ERA5	DL - ERA5	CFSv2 - ERA5	DL - ERA5	CFSv2 - ERA5
Hurricane Katrina	**-0.345**	8.839	**0.453**	12.18	**-0.811**	10.227
Hurricane Ivan	**-0.22**	8.466	**-0.036**	13.48	**-1.485**	13.135
Cyclone Nargis	**-5.37**	21.151	**-1.245**	43.845	**2.338**	47.233
Europe Floods	**-0.2**	6.654	**-0.015**	8.134	**0.12**	6.94
China Floods	**-0.17**	11.233	**0.465**	18.903	**-0.48**	16.877
India flood	**0.003**	17.321	**0.139**	25.297	**-0.749**	20.259

Table 2. Performance of the deep learning augmented numerical weather prediction system CFSv2 versus CFSv2 alone. The table shows regional bias/error in simulating various extreme precipitation events by the hybrid deep learning and CFSv2 system versus CFSv2 alone. The events occured as (i) Hurricane Katrina in 2005, (ii) Hurricane Ivan in 2004, (iii) Cyclone Nargis in 2008, (iv) Europe floods in 2010, (v) China flood in 2005 and (vi) India flood in 2005

Singh, M., Acharya, N., Grover, A., Rao, S.A., Kumar, B., Yang, Z.L. and Niyogi, D., Short-range forecasts of global precipitation using deep learning-augmented numerical weather prediction. *NeurIPS 2022*

From global to local weather prediction

We first need to develop supervised learning datasets. The solution is being provided by **DownScaleBench**

DownScaleBench for developing and applying a deep learning based urban climate downscaling

Singh, M., Acharya, N., Jamshidi, S., Jiao, J., Yang, Z.L., Coudert, M., Baumer, Z. and Niyogi, D., 2023. DownScaleBench for developing and applying a deep learning based urban climate downscaling-first results for high-resolution urban precipitation climatology over Austin, Texas. Computational Urban Science, 3(1), p.22.

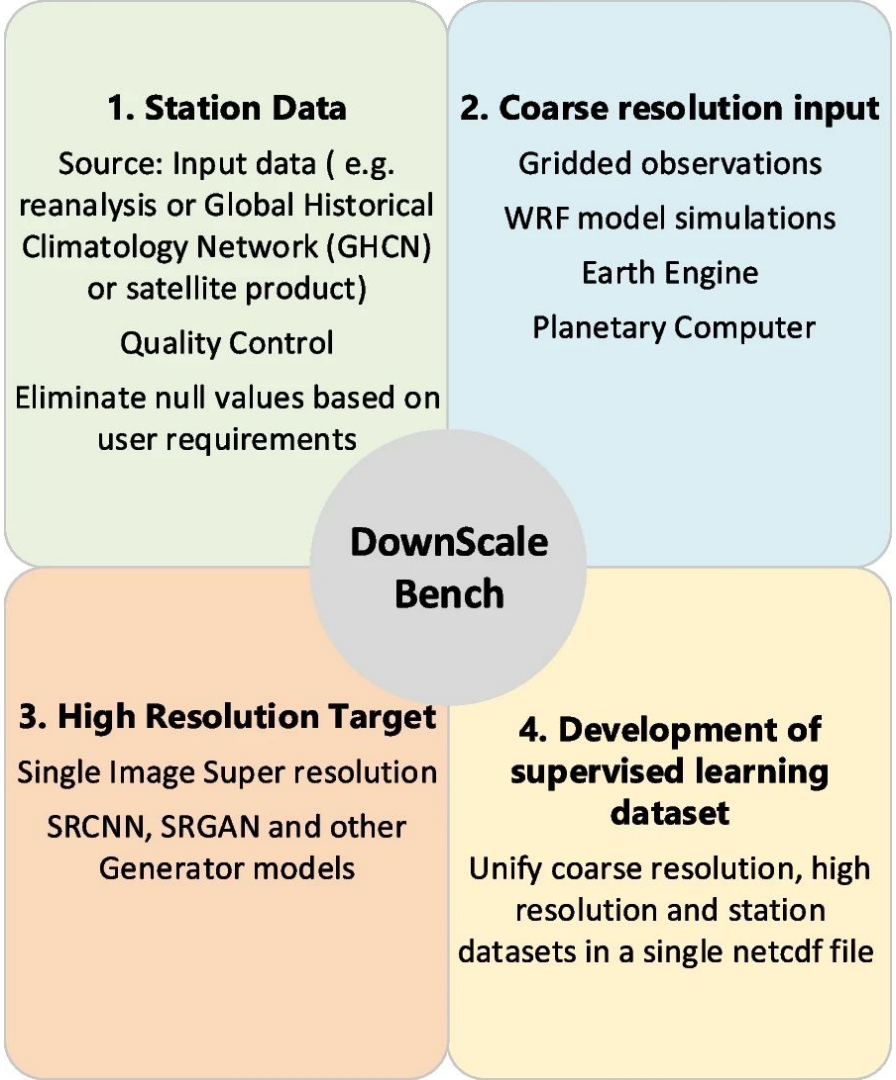

Singh, M., Acharya, N., Jamshidi, S., Jiao, J., Yang, Z.L., Coudert, M., Baumer, Z. and Niyogi, D., 2023. DownScaleBench for developing and applying a deep learning based urban climate downscaling-first results for high-resolution urban precipitation climatology over Austin, Texas. Computational Urban Science, 3(1), p.22.

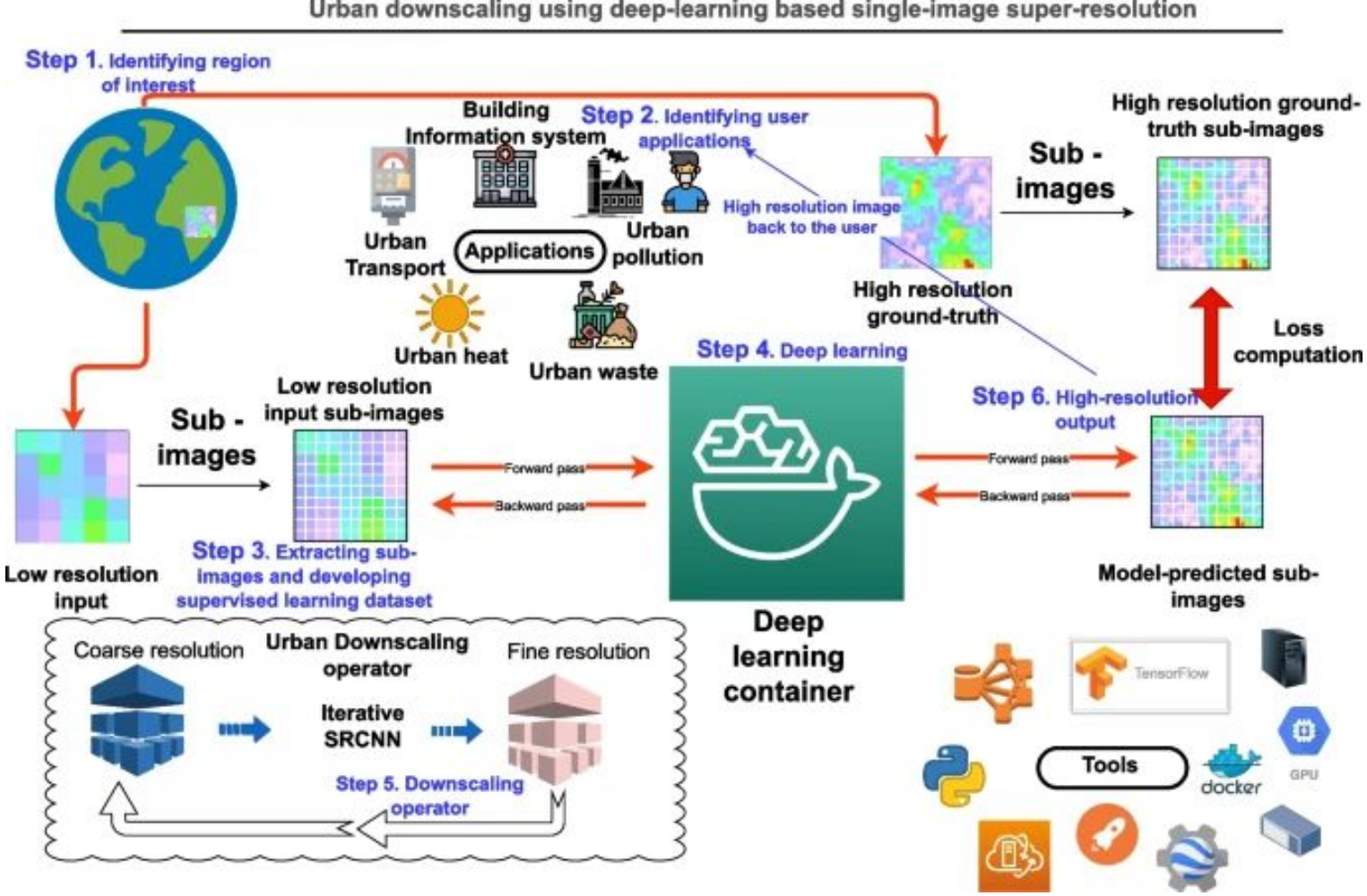

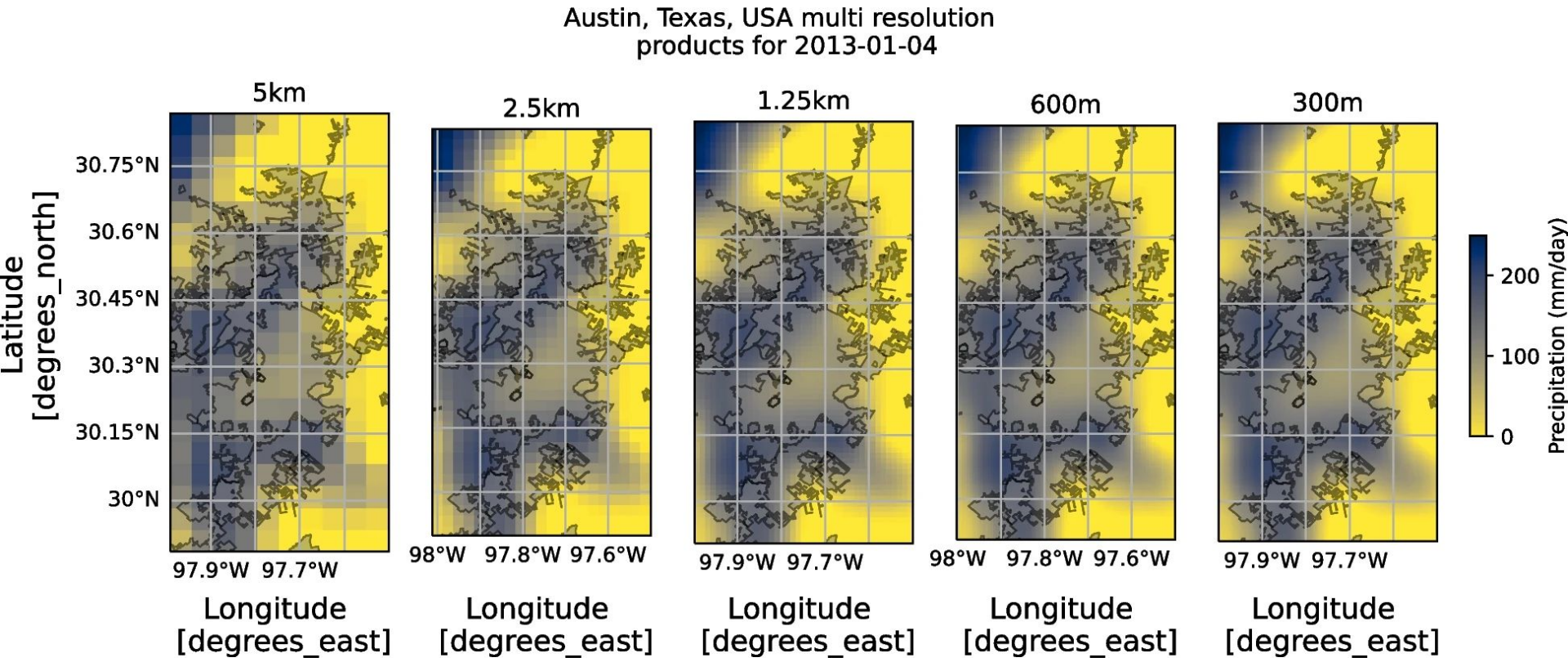

Singh, M., Acharya, N., Jamshidi, S., Jiao, J., Yang, Z.L., Coudert, M., Baumer, Z. and Niyogi, D., 2023. DownScaleBench for developing and applying a deep learning based urban climate downscaling-first results for high-resolution urban precipitation climatology over Austin, Texas. Computational Urban Science, 3(1), p.22.

Next, we need state of the art models to perform super-resolution/downscaling. The solution is being provided by **ClimateDownscaleSuite**

ClimateDownscaleSuite: Unifying deep learning models for weather and climate downscaling

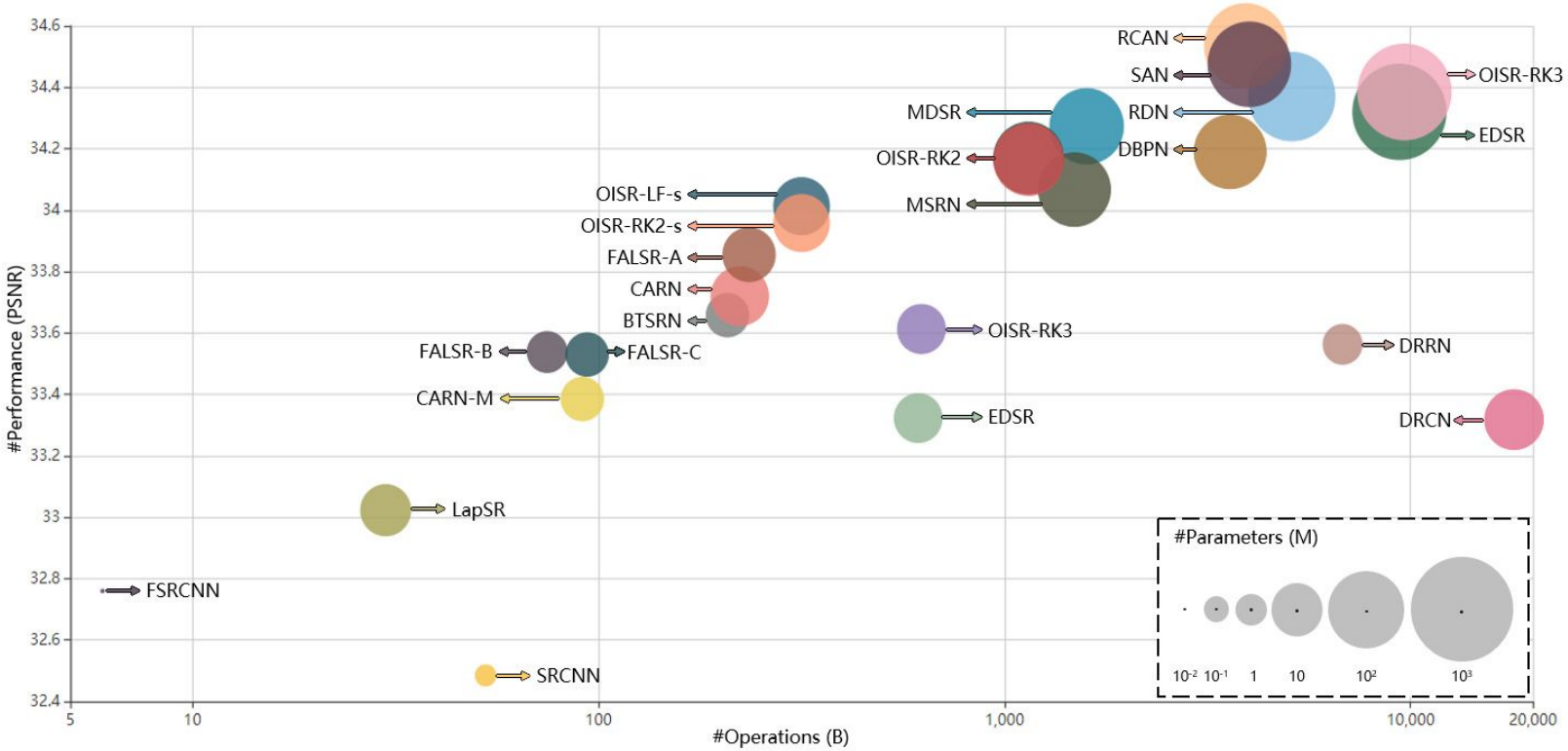

Singh et al, manuscript in preparation

ClimateDownscaleSuite

applied to VIIRS to DMSP night time lights data transformation

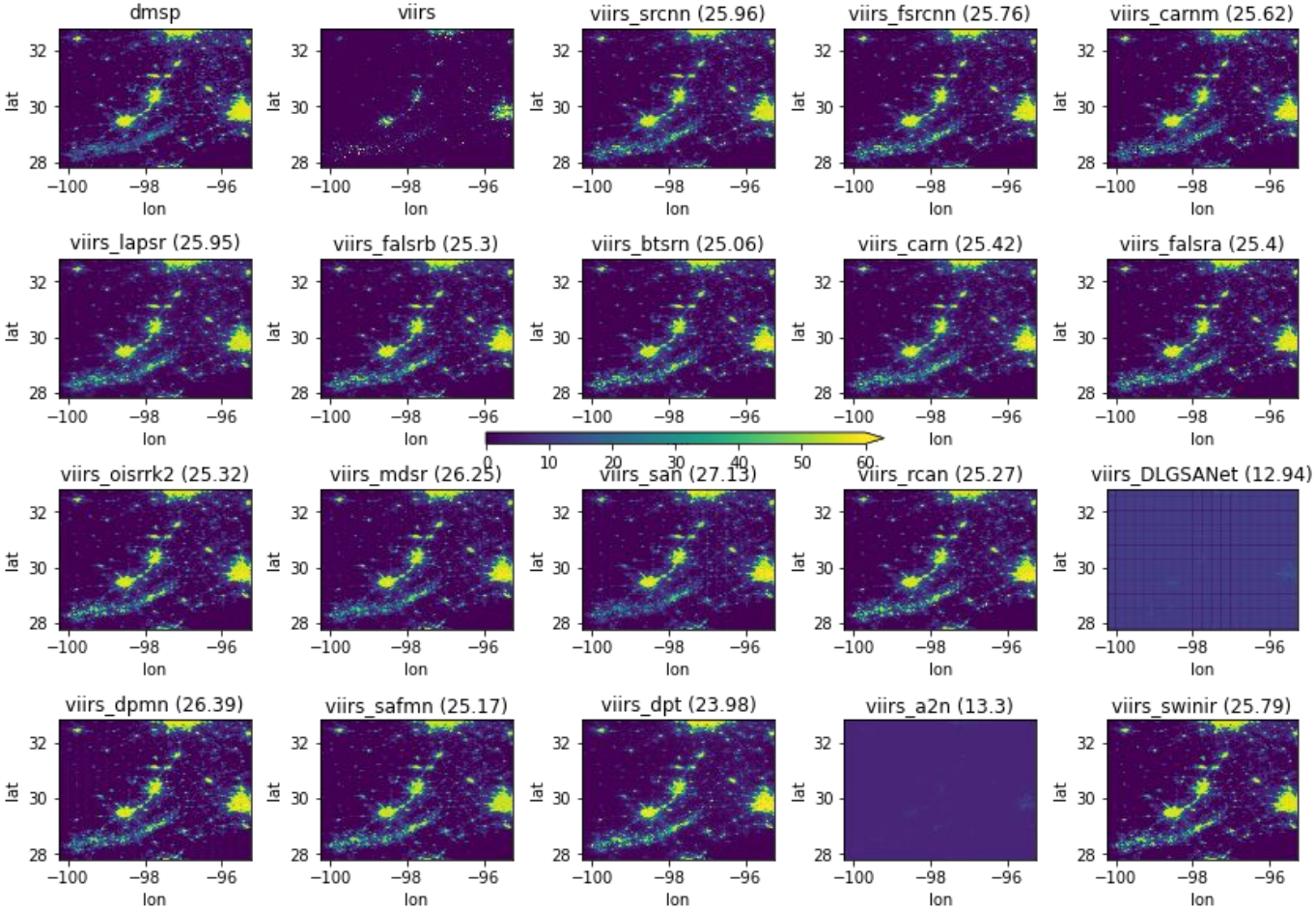

Singh et al, manuscript in preparation

We also need state of the art novel methods to fuse station datasets into downscaling algorithms **MeteoGAN is the answer**

MeteoGAN for urban digital twins

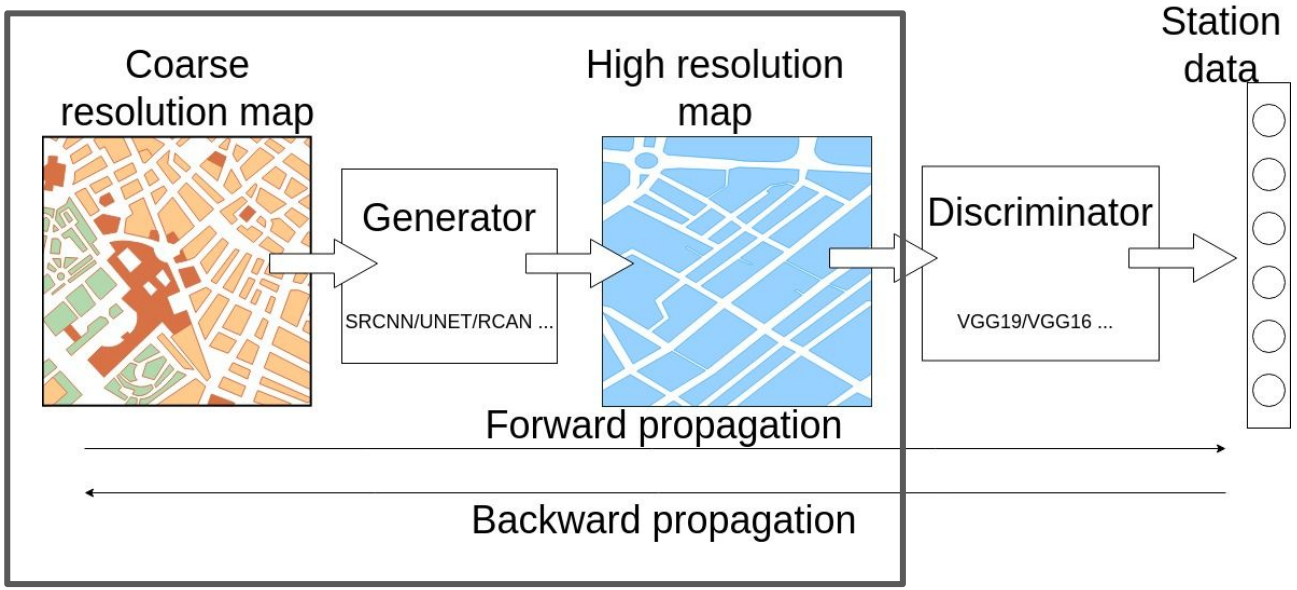

First results from MeteoGAN over Delhi, India

1993-09-10

CHIRPS (5 km)

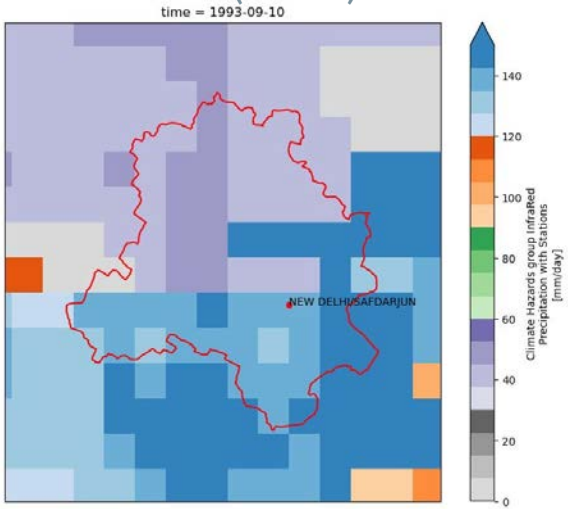

Bicubic (300 m)

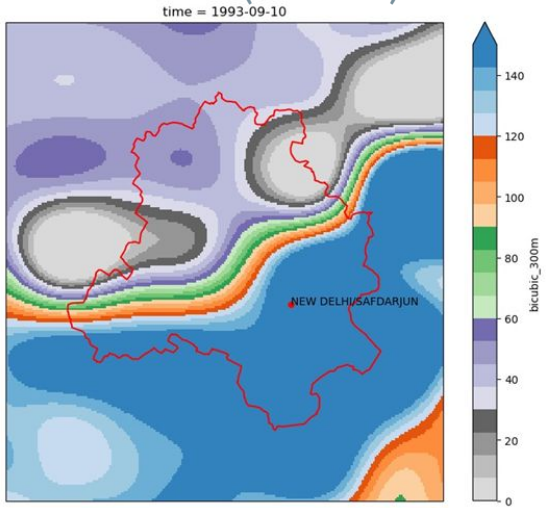

MeteoGAN (300 m)

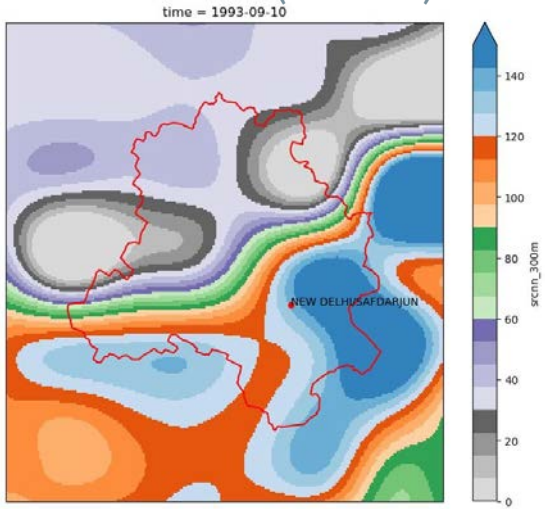

First results from MeteoGAN over Delhi, India

1988-08-19

CHIRPS (5 km)

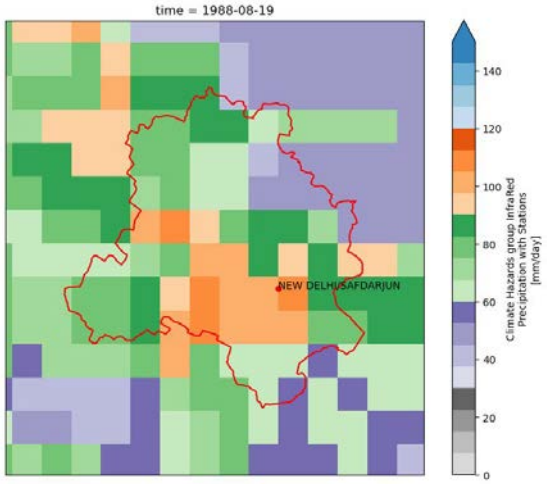

Bicubic (300 m)

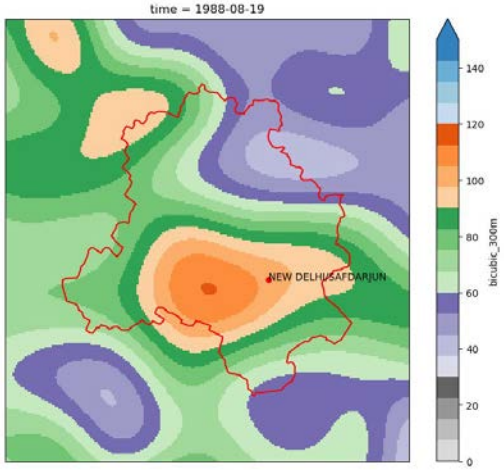

MeteoGAN (300 m)

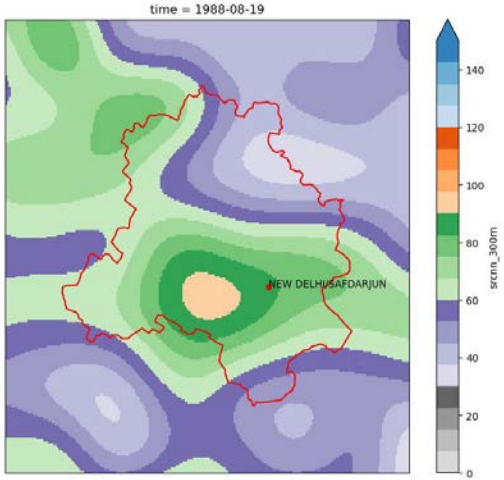

MeteoGAN based land surface temperature at 30-m

Incorporating physical boundary

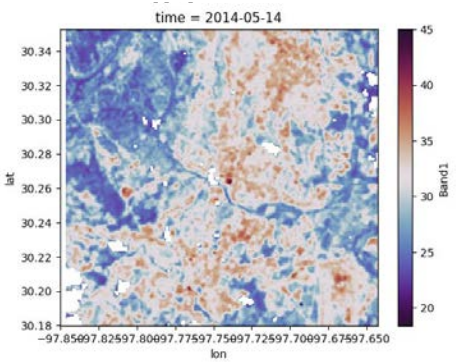

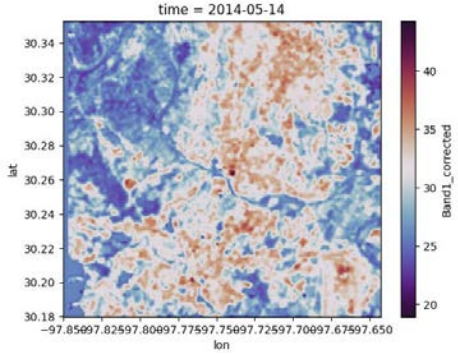

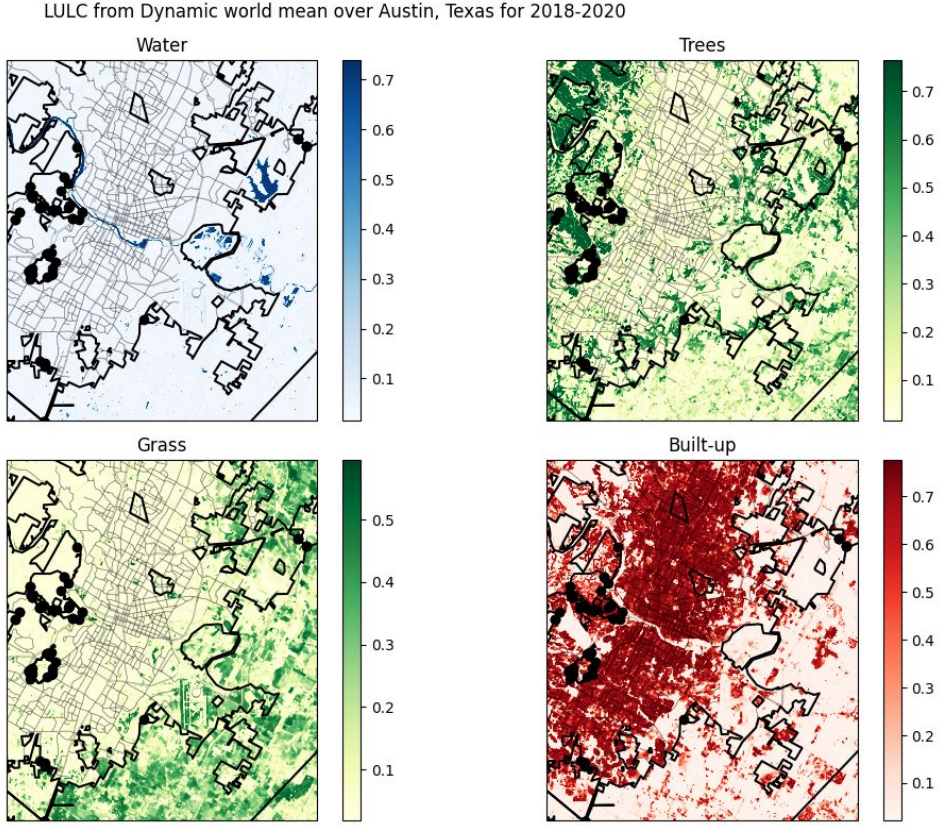

Pangu-Weather - 3D Earth Specific Transformer

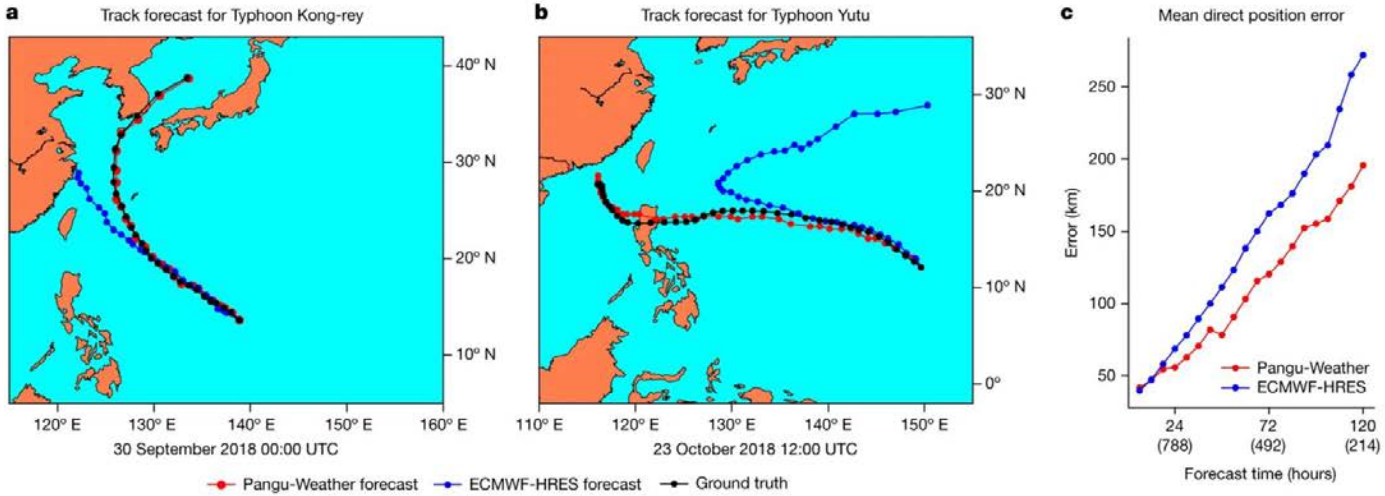

a,**b**, Tracking results for two strong tropical cyclones in 2018, that is, Typhoon Kong-rey (2018–25) and Yutu (2018–26). The initial time point is shown below each panel. The time gap between neighbouring dots is 6 h. Pangu-Weather forecasts the correct path of Yutu (that is, it goes to the Philippines) at 12:00 UTC on 23 October 2018, whereas ECMWF-HRES obtains the same conclusion 2 days later, before which it predicts that Yutu will make a big turn to the northeast. **c**, A comparison between Pangu-Weather and ECMWF-HRES in terms of mean direct position error over 88 cyclones in 2018. Each number in brackets in the *x*-axis indicates the number of samples used to calculate the average. For example, '(788)' means that there are in total 788 initial points from which the typhoon lasts for at least 24 hours, and the 788 direct position errors of Pangu-Weather and ECMWF-HRES were averaged into the final results. Panels **a** and **b** were plotted using the Matplotlib Basemap toolkit.

Bi, K., Xie, L., Zhang, H., Chen, X., Gu, X. and Tian, Q., 2023. Accurate medium-range global weather forecasting with 3D neural networks. *Nature*, *619*(7970), pp.533-538.

GraphCast

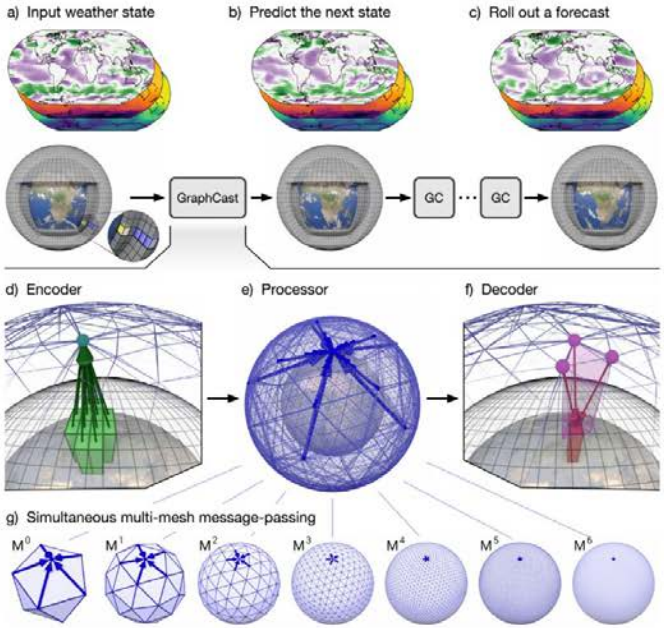

Figure 1 | **Model schematic.** (a) The input weather state(s) are defined on a 0.25° latitude-longitude grid comprising a total of 721 × 1440 = 1,038,240 points. Yellow layers in the closeup pop-out window represent the 5 surface variables, and blue layers represent the 6 atmospheric variables that are repeated at 37 pressure levels (5 + 6 × 37 = 227 variables per point in total), resulting in a state representation of 235,680,480 values. (b) GraphCast predicts the next state of the weather on the grid. (c) A forecast is made by iteratively applying

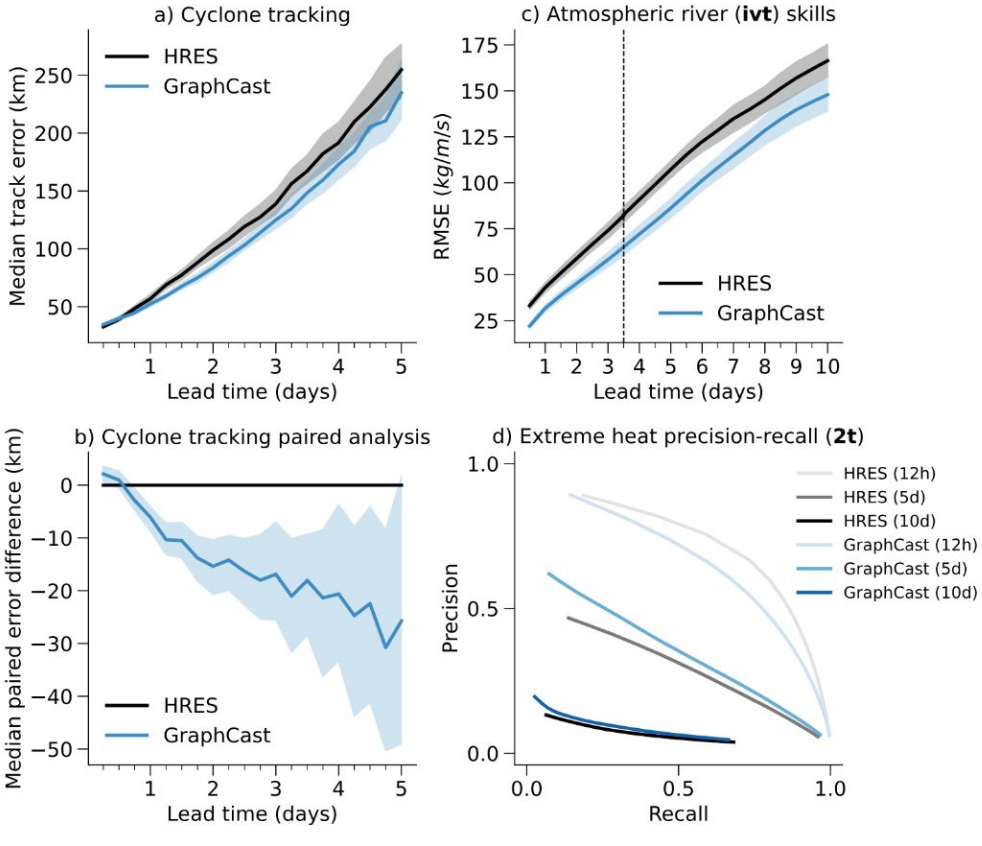

Lam, R., Sanchez-Gonzalez, A., Willson, M., Wirnsberger, P., Fortunato, M., Alet, F., Ravuri, S., Ewalds, T., Eaton-Rosen, Z., Hu, W. and Merose, A., 2023. Learning skillful medium-range global weather forecasting. *Science*, *382*(6677), pp.1416-1421.

Fourcastnet

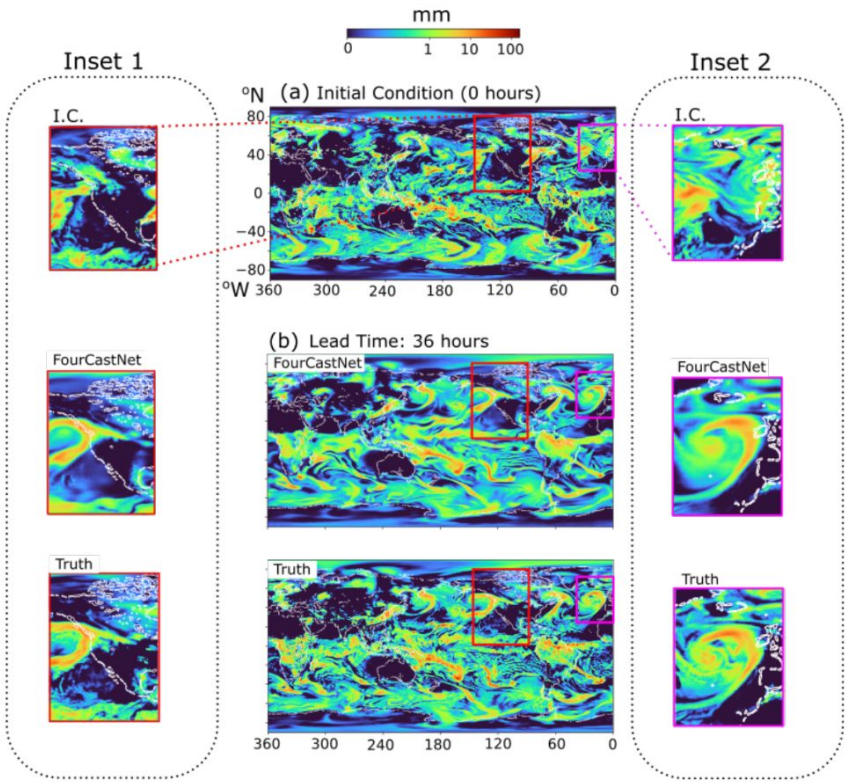

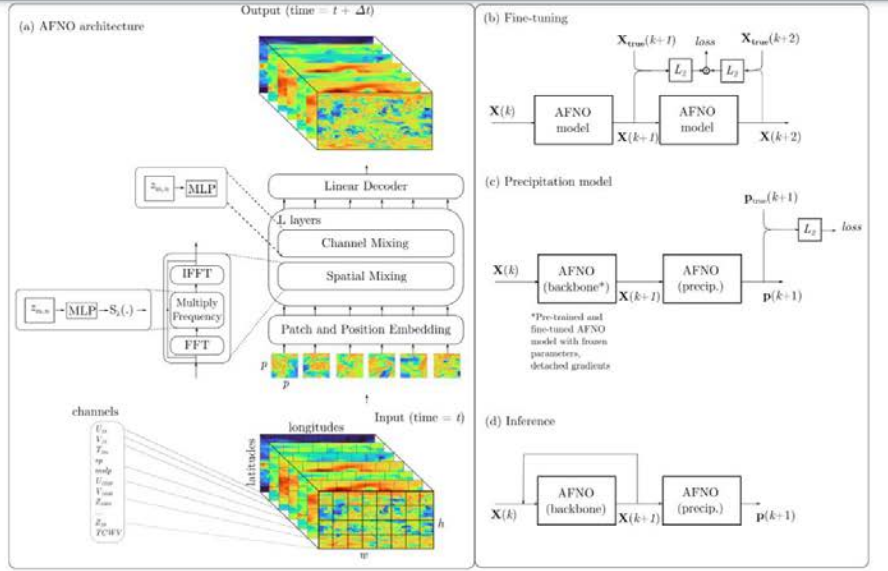

Figure 2: (a) The multi-layer transformer architecture that utilizes the Adaptive Fourier Neural Operator with shared MLP and frequency soft-thresholding for spatial token mixing. The input frame is first divided into a $h \times w$ grid of patches, where each patch has a small size $p \times p \times c$. Each patch is then embedded in a higher dimensional space with high number of latent channels and position embedding is added to form a sequence of tokens. Tokens are then mixed spatially using AFNO, and subsequently for each token the latent channels are mixed. This process is repeated for L layers, and finally a linear decoder reconstructs the patches for the next frame from the final embedding. The right-hand panels describe the FourCastNet model's additional training and inference modes: (b) two-step fine-tuning, (c) backbone model that forecasts the 20 variables in Table 1 with secondary precipitation diagnostic model (note that $\mathbf{p}(k+1)$ denotes the 6 hour accumulated total precipitation that falls between $k+1$ and $k+2$ time steps) (d) forecast model in free-running autoregressive inference mode.

Kurth, T., Subramanian, S., Harrington, P., Pathak, J., Mardani, M., Hall, D., Miele, A., Kashinath, K. and Anandkumar, A., 2023, June. Fourcastnet: Accelerating global high-resolution weather forecasting using adaptive fourier neural operators. In *Proceedings of the platform for advanced scientific computing conference* (pp. 1-11).

FuXi

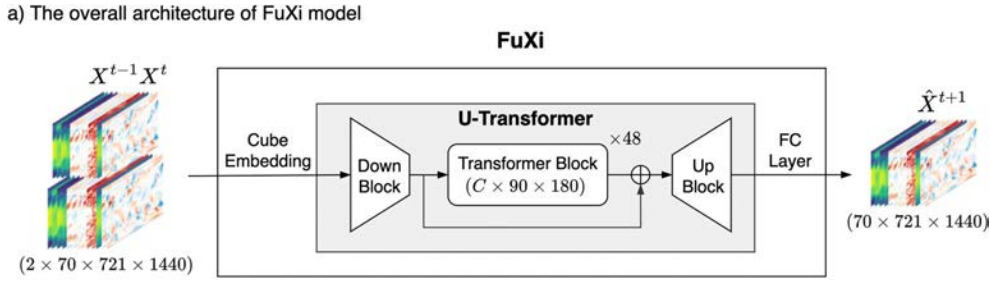

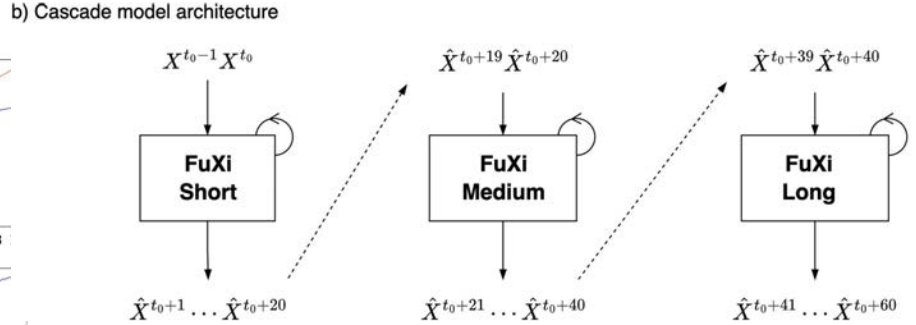

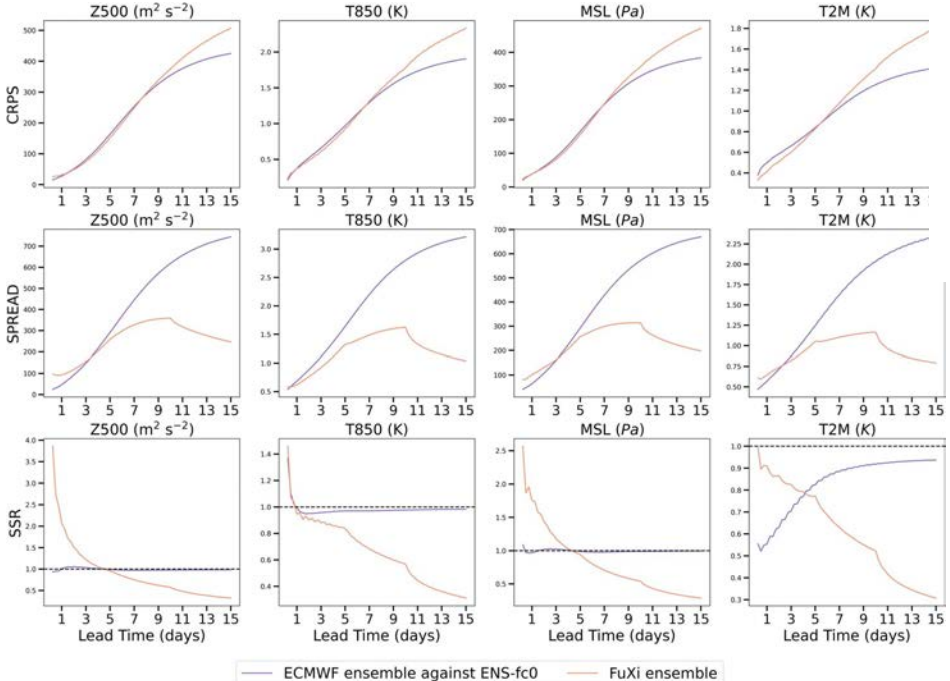

Chen, L., Zhong, X., Zhang, F., Cheng, Y., Xu, Y., Qi, Y. and Li, H., 2023. FuXi: a cascade machine learning forecasting system for 15-day global weather forecast. *npj Climate and Atmospheric Science*, *6*(1), p.190.

SwinRDM

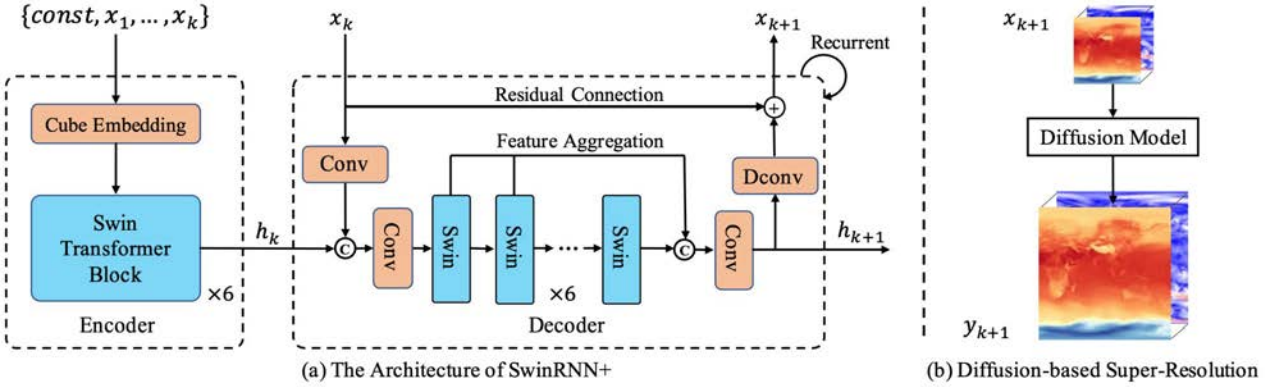

Figure 1: The SwinRDM consists of two parts: (a) the low-resolution forecasting model SwinRNN+ is an improved version of SwinRNN, which adopts a single-scale architecture and adds a multi-layer feature aggregation component, and (b) the diffusion-based super-resolution model conditions on the prediction x_{k+1} from SwinRNN+.

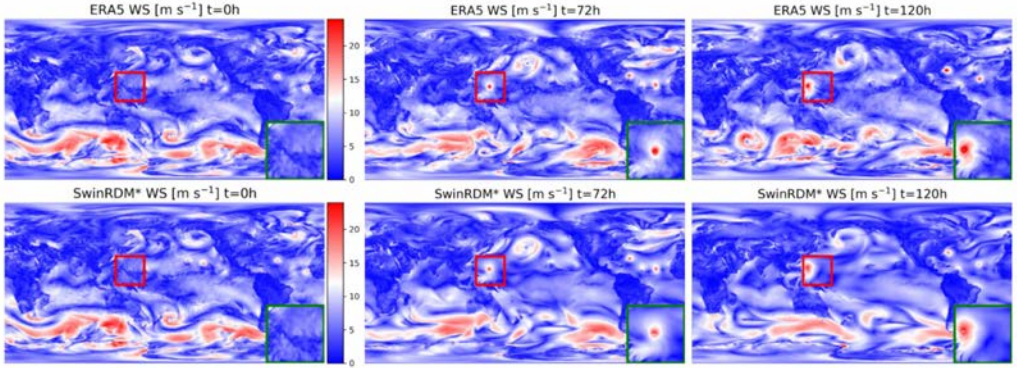

Figure 5: Qualitative illustration of a global near-surface wind forecast generated by our SwinRDM*. The prediction starts at the initial time of September 8, 2018, 06:00 UTC. The zoom-in area shows the beginning of Super Typhoon Mangkhut. Our method successfully forecasts Super Typhoon Mangkhut with high accuracy and rich fine-scale features.

Chen, L., Du, F., Hu, Y., Wang, Z. and Wang, F., 2023, June. Swinrdm: integrate swinrnn with diffusion model towards high-resolution and high-quality weather forecasting. In *Proceedings of the AAAI Conference on Artificial Intelligence* (Vol. 37, No. 1, pp. 322-330).

NeuralGCM

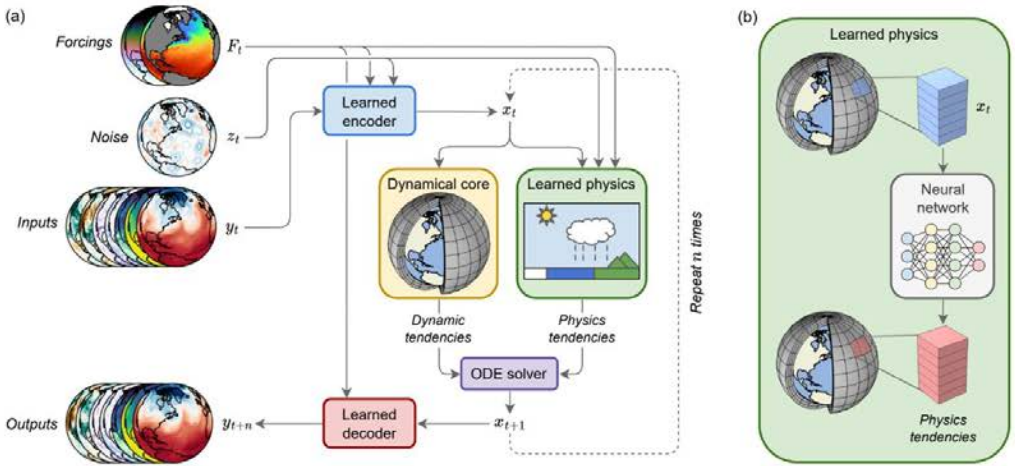

Fig. 1 Structure of the NeuralGCM model. (a) Overall model structure, showing how forcings F_t, noise z_t (for stochastic models), and inputs y_t are encoded into the model state x_t. Model state is fed into the dynamical core, and alongside forcings and noise into the learned physics module. This produces tendencies (rates of change) used by an implicit-explicit ODE solver to advance the state in time. The new model state x_{t+1} can then be fed back into another time step, or decoded into model predictions. (b) Inset of the learned physics module, which feeds data for individual columns of the atmosphere into a neural network used to produce physics tendencies in that vertical column.

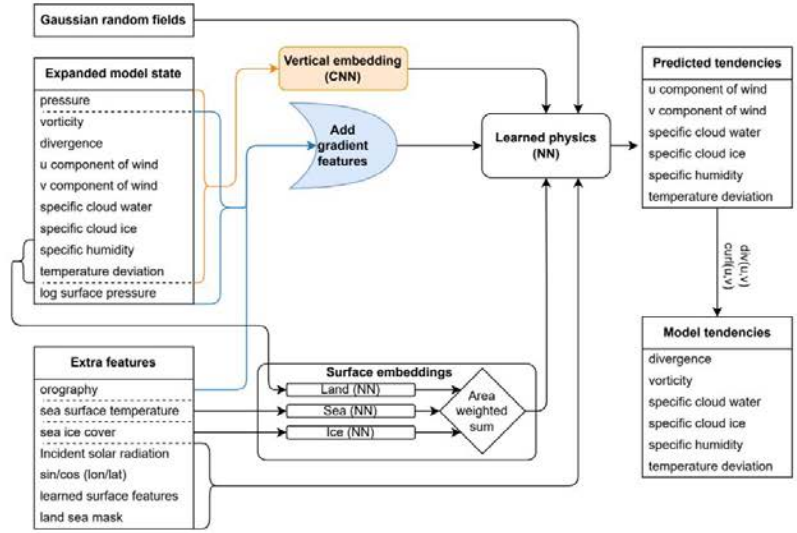

Fig. C5 Visualization of the data flow in the learned physics module of NeuralGCM.

Kochkov, D., Yuval, J., Langmore, I., Norgaard, P., Smith, J., Mooers, G., Lottes, J., Rasp, S., Düben, P., Klöwer, M. and Hatfield, S., 2023. Neural general circulation models. *arXiv preprint arXiv:2311.07222*.

Aurora

AURORA: A FOUNDATION MODEL OF THE ATMOSPHERE

Cristian Bodnar[*, 1], Wessel P. Bruinsma[*, 1], Ana Lucic[*, 1], Megan Stanley[*, 1], Johannes Brandstetter[3, †], Patrick Garvan[1], Maik Riechert[1], Jonathan Weyn[2], Haiyu Dong[2], Anna Vaughan[4], Jayesh K. Gupta[5, †], Kit Tambiratnam[2], Alex Archibald[4], Elizabeth Heider[1], Max Welling[6, †], Richard E. Turner[1, 4], and Paris Perdikaris[1]

[1]Microsoft Research AI for Science
[2]Microsoft Corporation [3]JKU Linz [4]University of Cambridge [5]Poly Corporation [6]University of Amsterdam

[*]Equal contribution [†]Work done while at Microsoft Research

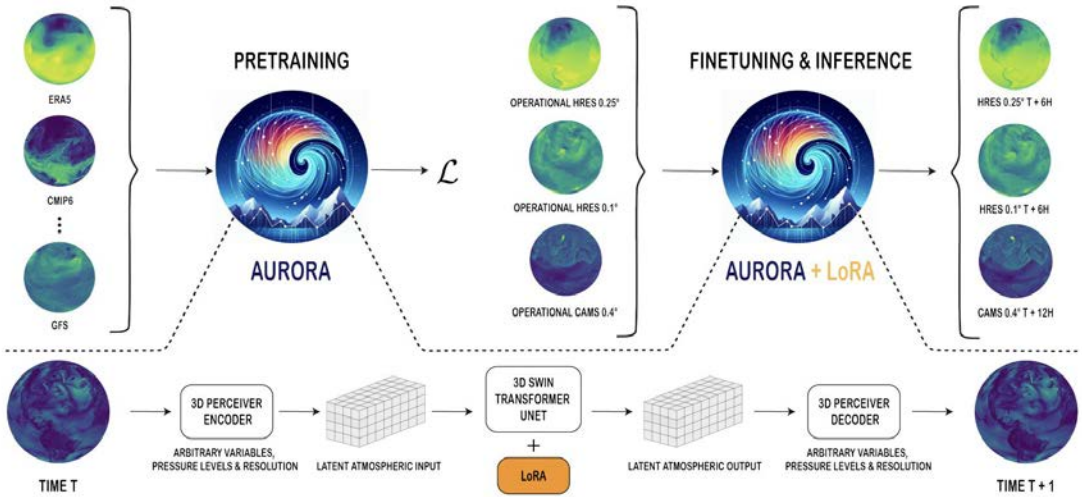

Figure 1: **Aurora is a 1.3 billion parameter foundation model for high-resolution forecasting of weather and atmospheric processes.** Aurora is a flexible 3D Swin Transformer with 3D Perceiver-based encoders and decoders. At pretraining time, Aurora is optimised to minimise a loss $\mathcal{L}$ on multiple heterogeneous datasets with different resolutions, variables, and pressure levels. The model is then fine-tuned in two stages: (1) short-lead time fine-tuning of the pretrained weights (2) long-lead time (rollout) fine-tuning using Low Rank Adaptation (LoRA). The fine-tuned models are then deployed to tackle a diverse collection of operational forecasting scenarios at different resolutions.

StormCast

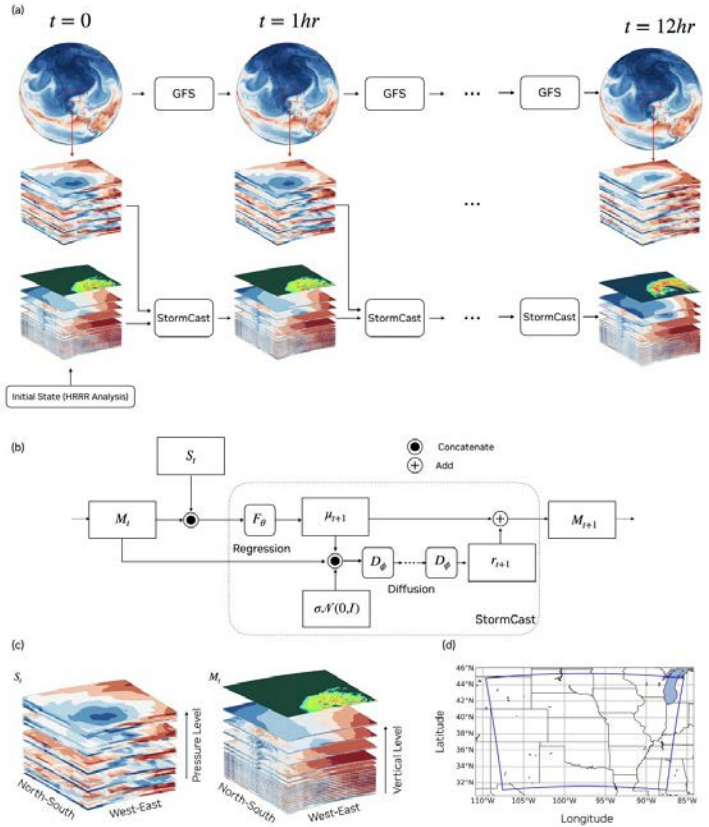

Kilometer-Scale Convection Allowing Model Emulation using Generative Diffusion Modeling

Jaideep Pathak*[1], Yair Cohen*[1], Piyush Garg*[1], Peter Harrington*[2], Noah Brenowitz[1], Dale Durran[1,3], Morteza Mardani[1], Arash Vahdat[1], Shaoming Xu†[4], Karthik Kashinath[1], Michael Pritchard[1]

August 21, 2024

[1]NVIDIA Corporation
[2]Lawrence Berkeley National Laboratory
[3]University of Washington
[4]University of Minnesota
*Equal Contribution

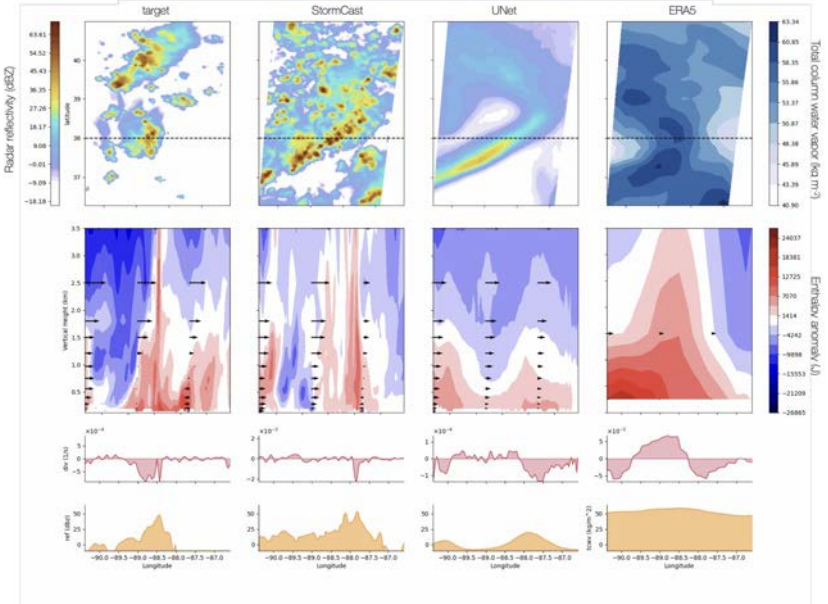

DIFFOBS: GENERATIVE DIFFUSION FOR GLOBAL FORECASTING OF SATELLITE OBSERVATIONS

Jason Stock*
NVIDIA Corporation and Colorado State University
stock@colostate.edu

Jaideep Pathak, Yair Cohen, Mike Pritchard, Piyush Garg, Dale Durran, Morteza Mardani & Noah Brenowitz
NVIDIA Corporation
{jpathak,yacohen,mpritchard,piyushg,ddurran,
mmardani,nbrenowitz}@nvidia.com

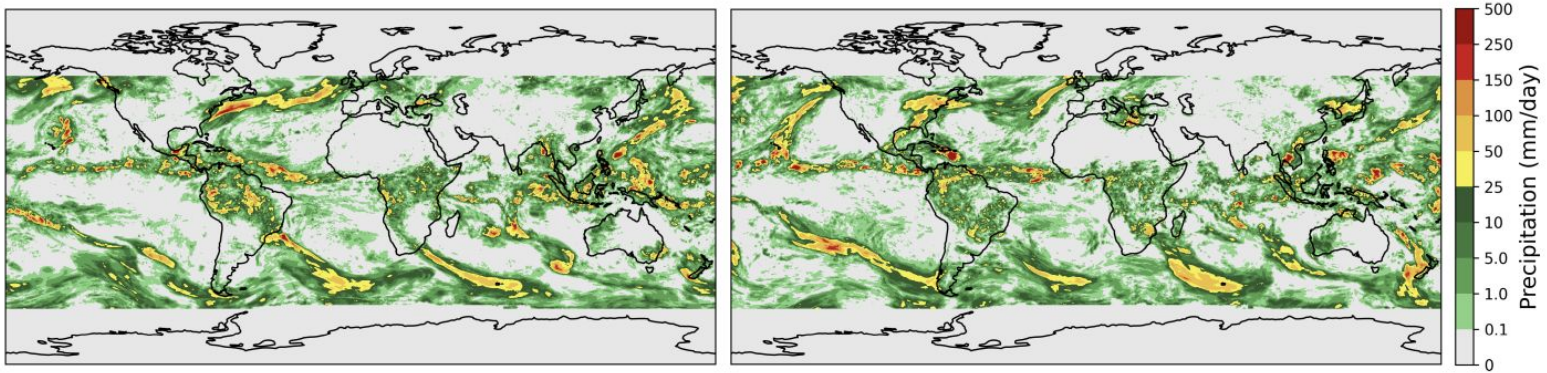

(a) Observation (b) DiffObs

Figure 1: Example 3-day rollout from Oct 27, 2020 as initial condition.

Weatherbench-2

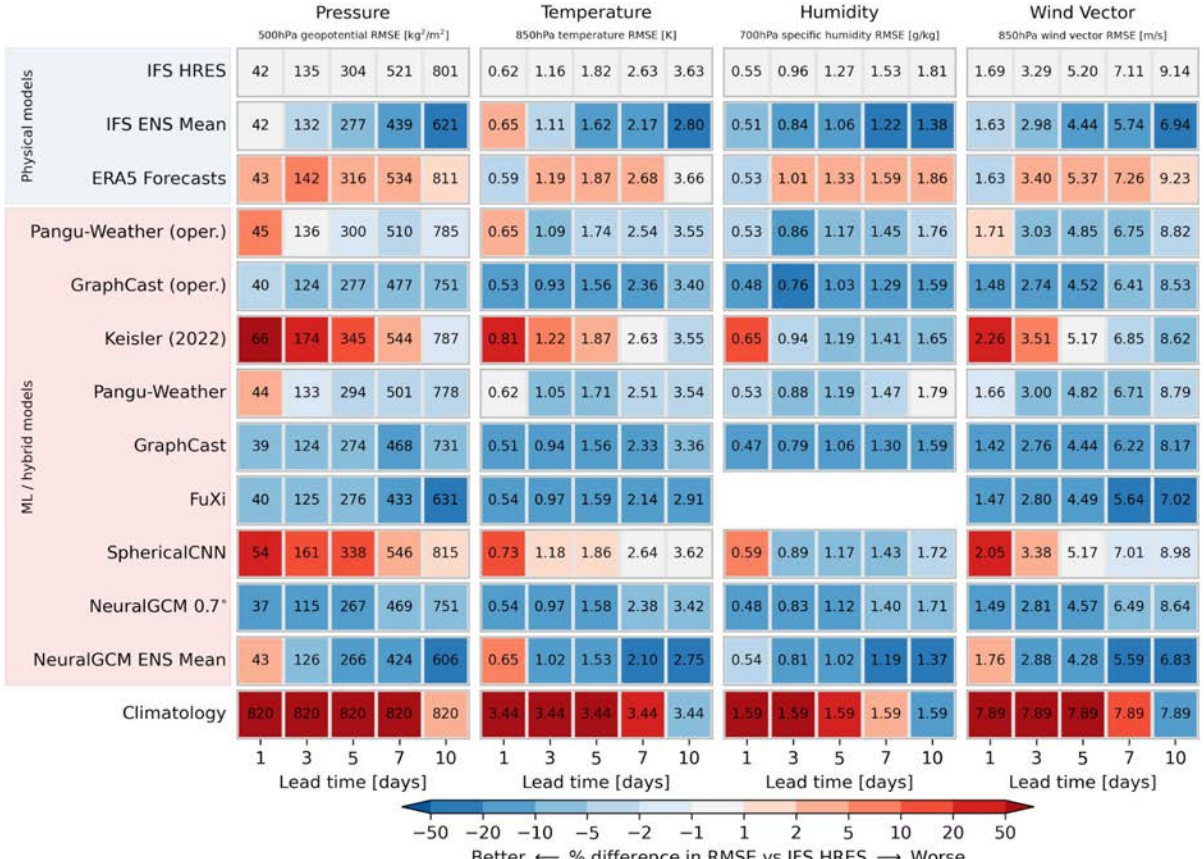

Rasp, S., Hoyer, S., Merose, A., Langmore, I., Battaglia, P., Russel, T., Sanchez-Gonzalez, A., Yang, V., Carver, R., Agrawal, S. and Chantry, M., 2023. Weatherbench 2: A benchmark for the next generation of data-driven global weather models. *arXiv preprint arXiv:2308.15560*.

Weatherbench-2

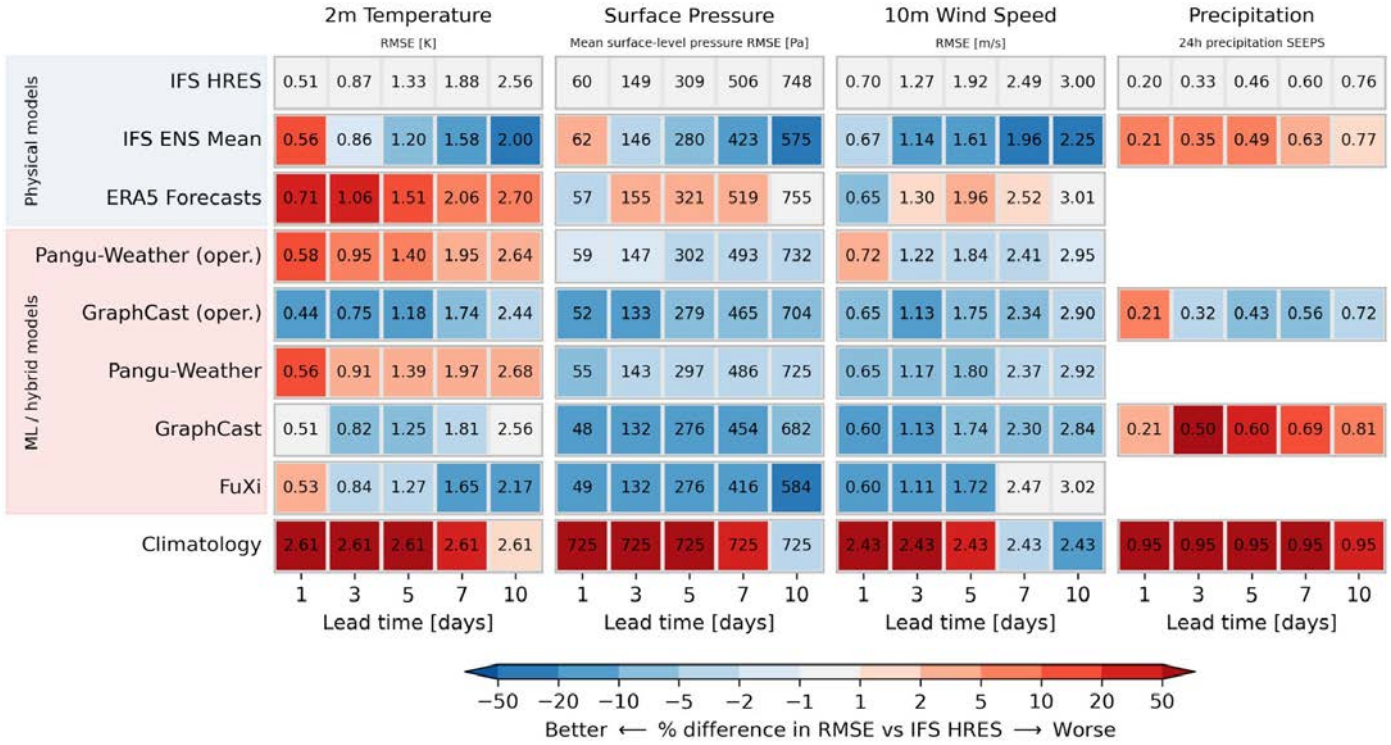

Rasp, S., Hoyer, S., Merose, A., Langmore, I., Battaglia, P., Russel, T., Sanchez-Gonzalez, A., Yang, V., Carver, R., Agrawal, S. and Chantry, M., 2023. Weatherbench 2: A benchmark for the next generation of data-driven global weather models. *arXiv preprint arXiv:2308.15560*.

HealPix

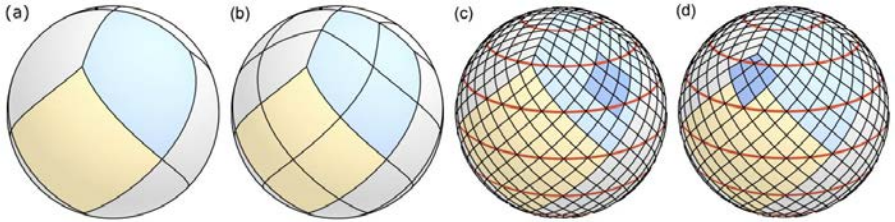

Figure 1: Division of the sphere into twelve faces according to the HEALPix. Four faces to represent either the northern (blue) and southern extratropics, while four more faces arrange around the equator to represent the tropics (yellow). Each face can be subdivided into patches with divisions along the side of each face given by powers of two. The sphere in (a) has a pixel-count of one per face side; we call it `hpx1`. The sphere in (b) counts two pixels per side (`hpx2`), whereas the two spheres in (c) and (d) have eight pixels per side, i.e., `hpx8`. Several latitude lines in red emphasize the iso-latitudinal arrangement of the patches. The saturated blue area depicts a 3×3 stencil, as applied by a standard convolution. To apply the 3×3 stencil at the top corner of the equatorial faces, i.e., stencil position in (d), we fill in the missing corner patch with the average of the values in the two adjacent patches on the extratropical faces.

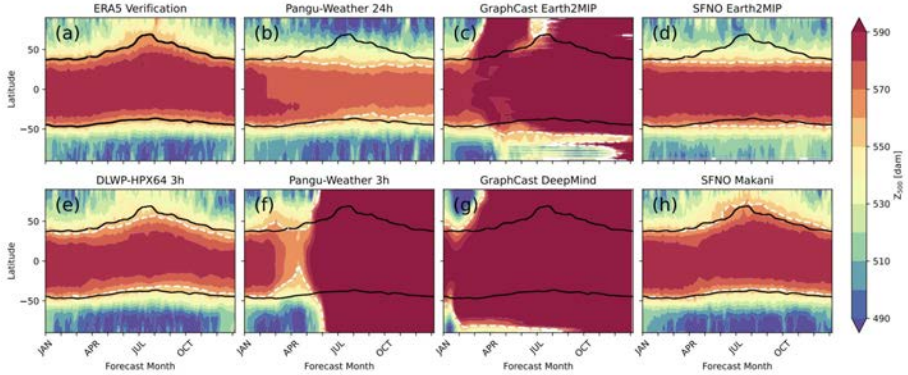

Figure 8: Zonally averaged three-day mean of Z_{500} plotted as a function of time and latitude: (a) for ERA5 reanalysis, (b)-(h) for recursive one-year simulations for each model as identified in the titles, initialized on January 2, 2018. Also shown are 15-day averaged values of the 5600 m contour of Z_{500} for the ERA5 data (black lines) each model simulation (white dashed lines).

Karlbauer, M., Cresswell-Clay, N., Durran, D.R., Moreno, R.A., Kurth, T., Bonev, B., Brenowitz, N. and Butz, M.V., 2024. Advancing parsimonious deep learning weather prediction using the HEALPix mesh. *Journal of Advances in Modeling Earth Systems*, *16*(8), p.e2023MS004021.

Coupled Ocean-Atmosphere Dynamics in a Machine Learning Earth System Model

Chenggong Wang *† Princeton University

Michael S. Pritchard * NVIDIA

Noah Brenowitz NVIDIA

Yair Cohen NVIDIA

Boris Bonev NVIDIA

Thorsten Kurth NVIDIA

Dale Durran University of Washington NVIDIA

Jaideep Pathak * NVIDIA

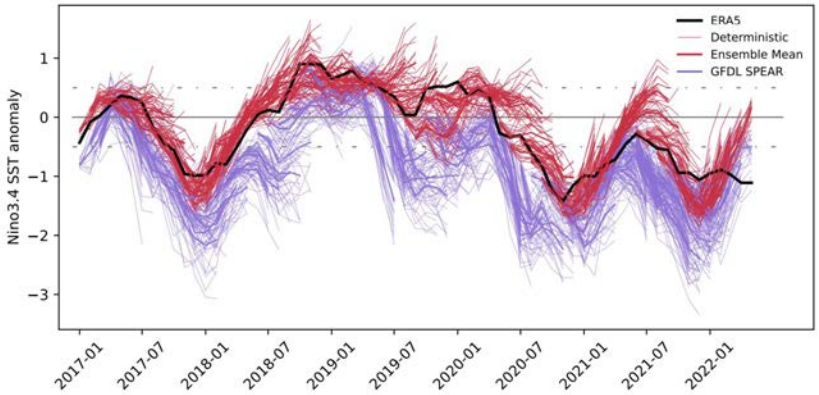

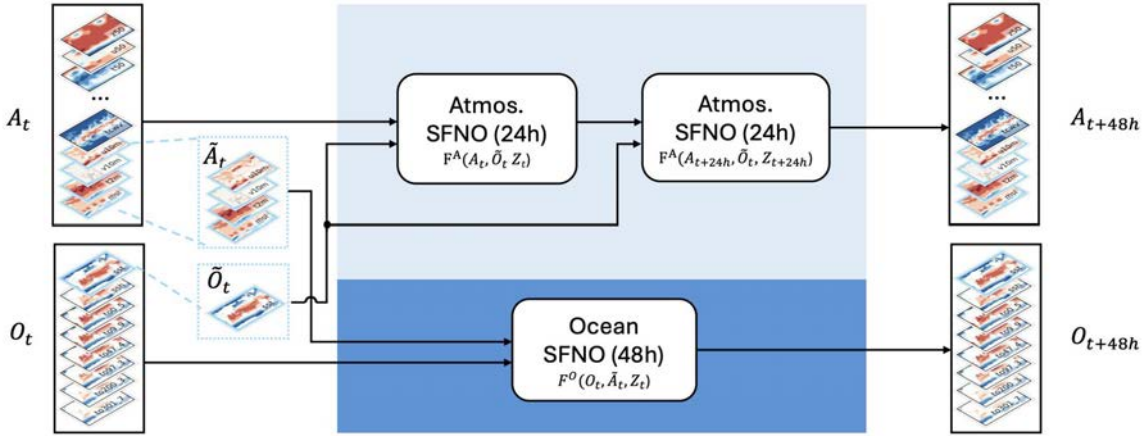

Fuxi-S2S

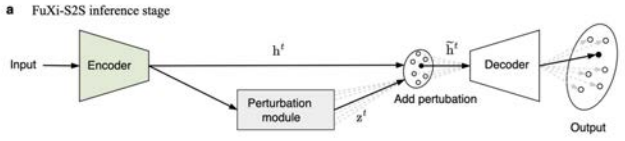

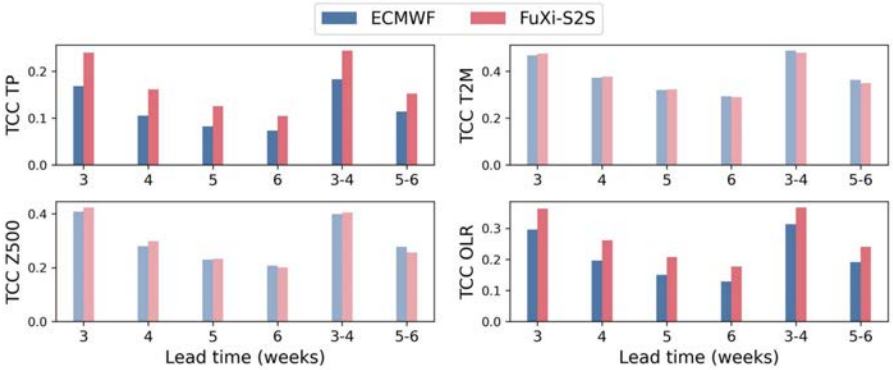

nature communications

Article

https://doi.org/10.1038/s41467-024-50714-1

A machine learning model that outperforms conventional global subseasonal forecast models

Received: 7 February 2024

Accepted: 19 July 2024

Published online: 30 July 2024

Check for updates

Lei Chen[1,2,10], Xiaohui Zhong[1,10], Hao Li[1,10] ✉, Jie Wu[3,10], Bo Lu[3,4] ✉, Deliang Chen[5], Shang-Ping Xie[6], Libo Wu[7,8,9], Qingchen Chao[3], Chensen Lin[1], Zixin Hu[1] & Yuan Qi[1,2] ✉

Skillful subseasonal forecasts are crucial for various sectors of society but pose a grand scientific challenge. Recently, machine learning-based weather forecasting models outperform the most successful numerical weather predictions generated by the European Centre for Medium-Range Weather Forecasts (ECMWF), but have not yet surpassed conventional models at subseasonal timescales. This paper introduces FuXi Subseasonal-to-Seasonal (FuXi-S2S), a machine learning model that provides global daily mean forecasts up to 42 days, encompassing five upper-air atmospheric variables at 13 pressure levels and 11 surface variables. FuXi-S2S, trained on 72 years of daily statistics from ECMWF ERA5 reanalysis data, outperforms the ECMWF's state-of-the-art Subseasonal-to-Seasonal model in ensemble mean and ensemble forecasts for total precipitation and outgoing longwave radiation, notably enhancing global precipitation forecast. The improved performance of FuXi-S2S can be primarily attributed to its superior capability to capture forecast uncertainty and accurately predict the Madden-Julian Oscillation (MJO), extending the skillful MJO prediction from 30 days to 36 days. Moreover, FuXi-S2S not only captures realistic teleconnections associated with the MJO but also emerges as a valuable tool for discovering precursor signals, offering researchers insights and potentially establishing a new paradigm in Earth system science research.

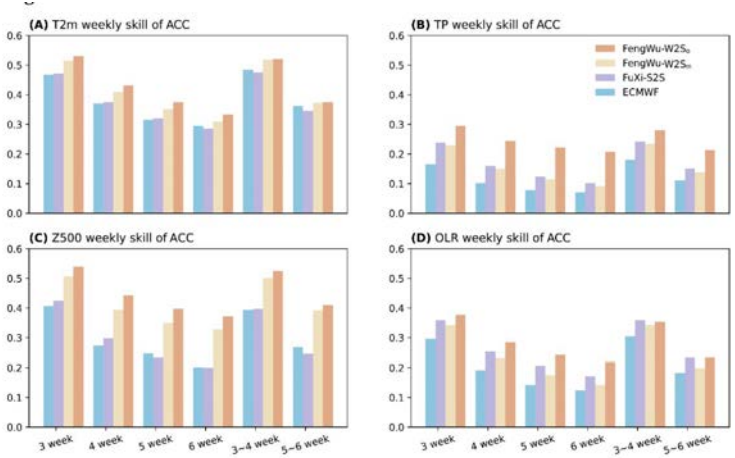

Figure 1 Correlation skills of subseasonal predictions among different models. (A) Predictive skill of 2m air temperature (T2m) anomalies as a function of lead week based on ECMWF (blue bar), Fuxi-S2S (purple bar) and FengWu-W2S forecasts. The skills of FengWu-W2S are assessed based on the anomalies calculated relative to the observed climatology (orange bar) and FengWu-W2S's hindcast climatology (yellow bar), respectively. The prediction skill is validated for the period of 2017–2021. (B, C, D) As in (A), but for the prediction skills of the anomalies of total precipitation (TP), T2m, and geopotential height at 500 hPa (Z500), respectively.

FengWu-W2S: A deep learning model for seamless weather-to-subseasonal forecast of global atmosphere

Authors: Fenghua Ling[1†], Kang Chen[1†], Jiye Wu[2†], Tao Han[1], Jing-Jia Luo[2*], Wanli Ouyang[1], Lei Bai[1*]

Affiliations:

[1]Shanghai AI Laboratory, Shanghai, China

[2]Institute for Climate and Application Research (ICAR)/ /School of Future Technology /CIC-FEMD, Nanjing University of Information Science and Technology, Nanjing, China

†Equal Contributions,

*Corresponding to baisanshi@gmail.com; jjluo@nuist.edu.cn

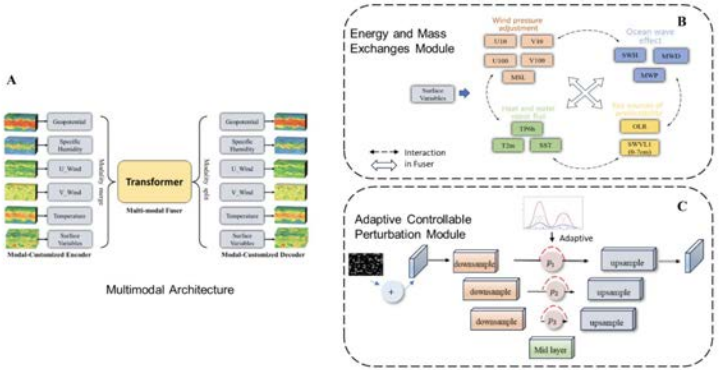

Supplementary Figure 1. The main components of FengWu-W2S. (A) The multimodal architecture of FengWu-W2S, which inherited from FengWu. (B) The surface data is divided into different modules for feature extract and facilitating the exchange of mass and energy between subsystem in the multi-modal fuser by a physically guided way. (C) Multi-level perturbation strategies for different variables that can be controlled manually.

AIFS-CRPS

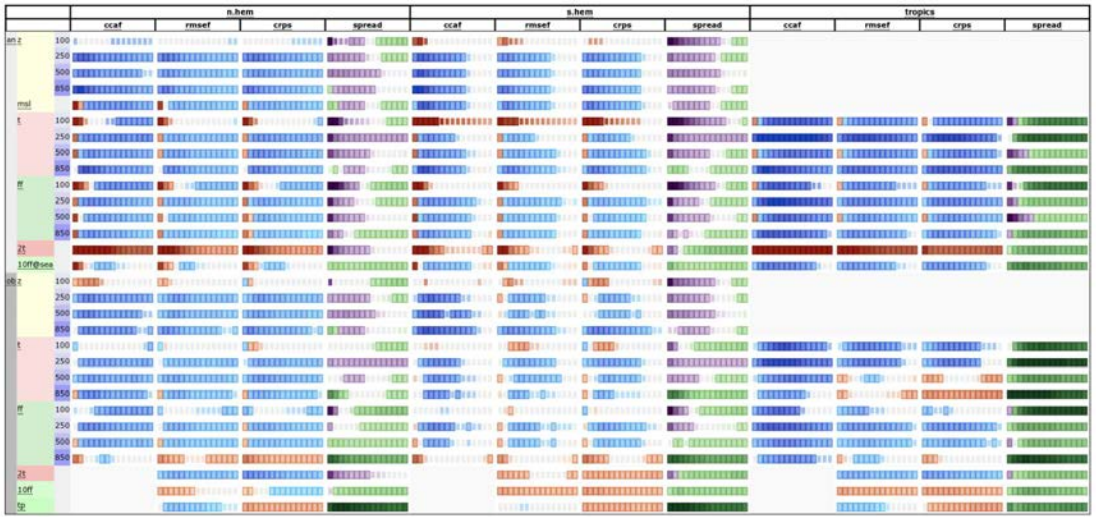

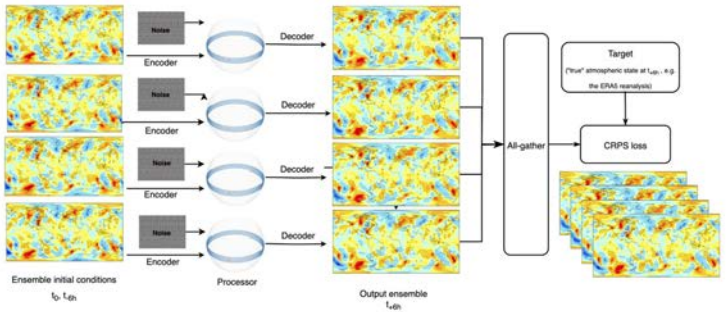

Figure 6: Scorecard comparing forecast scores of AIFS-CRPS O96 ensemble (approximately 1.0° spatial resolution) versus the IFS ensemble (approximately 0.1° spatial resolution), 1 February to 30 September 2024. Forecasts are initialised at 00 and 12 UTC. Shown are relative score changes as function of lead time (day 1 to 15) for northern extra-tropics (n.hem), southern extra-tropics (s.hem) and tropics. Blue colours mark score improvements and red colours score degradations. Purple colours indicate an increase in ensemble standard deviation, while green colours indicate a reduction. Differences that reach 95 % significance level are shown in light shading and differences that reach 99.7 % significance level are shown in dark shading. Variables are geopotential (z), temperature (t), wind speed (ff), mean sea level pressure (msl), 2 m temperature (2t), 10 m wind speed (10ff) and 24 hr total precipitation (tp). Numbers behind variable abbreviations indicate variables on pressure levels (e.g., 500 hPa), and prefix indicates verification against IFS NWP analyses (an) or radiosonde and SYNOP observations (ob). Scores shown are ensemble mean anomaly correlation

AI Quest

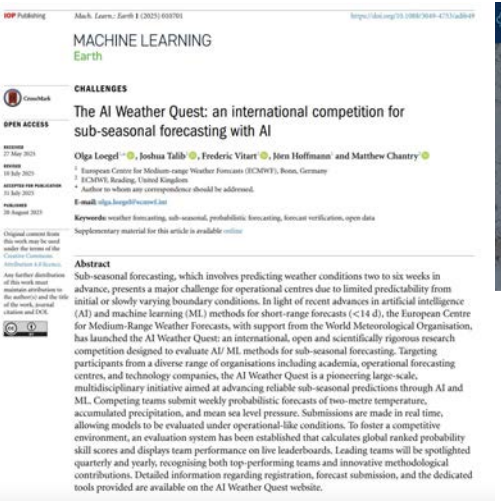

MACHINE LEARNING
Earth

CHALLENGES

The AI Weather Quest: an international competition for sub-seasonal forecasting with AI

Olga Loegel[1], Joshua Talib[1], Frederic Vitart[2], Jörn Hoffmann[1] and Matthew Chantry[2]

[1] European Centre for Medium-range Weather Forecasts (ECMWF), Bonn, Germany
[2] ECMWF, Reading, United Kingdom
* Author to whom any correspondence should be addressed.

E-mail: olga.loegel@ecmwf.int

Keywords: weather forecasting, sub-seasonal, probabilistic forecasting, forecast verification, open data

Supplementary material for this article is available online

OPEN ACCESS

RECEIVED 27 May 2025
REVISED 10 July 2025
ACCEPTED FOR PUBLICATION 31 July 2025
PUBLISHED 28 August 2025

Original content from this work may be used under the terms of the Creative Commons Attribution 4.0 licence.

Any further distribution of this work must maintain attribution to the author(s) and the title of the work, journal citation and DOI.

Abstract

Sub-seasonal forecasting, which involves predicting weather conditions two to six weeks in advance, presents a major challenge for operational centres due to limited predictability from initial or slowly varying boundary conditions. In light of recent advances in artificial intelligence (AI) and machine learning (ML) methods for short-range forecasts (<14 d), the European Centre for Medium-Range Weather Forecasts, with support from the World Meteorological Organisation, has launched the AI Weather Quest: an international, open and scientifically rigorous research competition designed to evaluate AI/ ML methods for sub-seasonal forecasting. Targeting participants from a diverse range of organisations including academia, operational forecasting centres, and technology companies, the AI Weather Quest is a pioneering large-scale, multidisciplinary initiative aimed at advancing reliable sub-seasonal predictions through AI and ML. Competing teams submit weekly probabilistic forecasts of two-metre temperature, accumulated precipitation, and mean sea level pressure. Submissions are made in real time, allowing models to be evaluated under operational-like conditions. To foster a competitive environment, an evaluation system has been established that calculates global ranked probability skill scores and displays team performance on live leaderboards. Leading teams will be spotlighted quarterly and yearly, recognising both top-performing teams and innovative methodological contributions. Detailed information regarding registration, forecast submission, and the dedicated tools provided are available on the AI Weather Quest website.

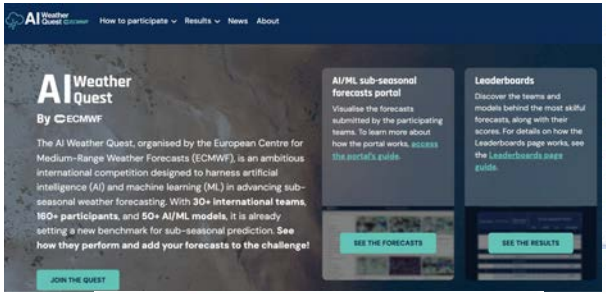

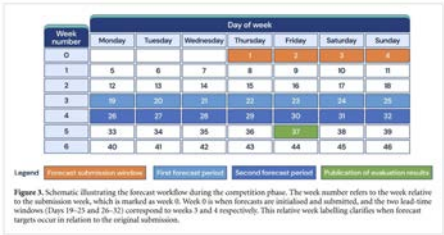

Week number	Day of week						
	Monday	Tuesday	Wednesday	Thursday	Friday	Saturday	Sunday
0				1	2	3	4
1	5	6	7	8	9	10	11
2	12	13	14	15	16	17	18
3	19	20	21	22	23	24	25
4	26	27	28	29	30	31	32
5	33	34	35	36	37	38	39
6	40	41	42	43	44	45	46

Legend: Forecast submission window | First forecast period | Second forecast period | Publication of evaluation results

Figure 3. Schematic illustrating the forecast workflow during the competition phase. The week number refers to the week relative to the submission week, which is marked as week 0. Week 0 is when forecasts are initialised and submitted, and the two lead-time windows (Days 19–25 and 26–32) correspond to weeks 3 and 4 respectively. This relative week labelling clarifies when forecast targets occur in relation to the original submission.

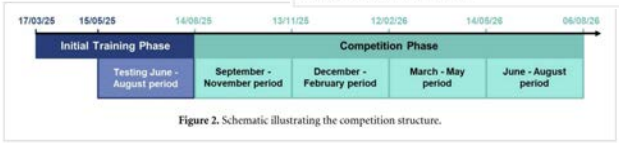

Figure 2. Schematic illustrating the competition structure.

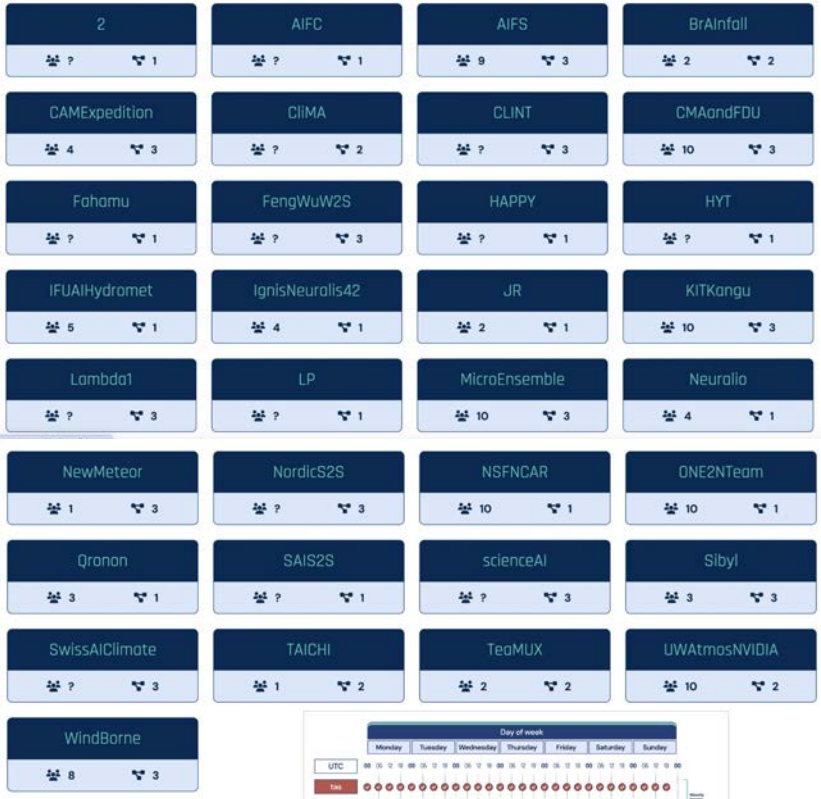

Figure 4. Schematic illustrating the data sampling frequency for tas, mslp, and pr.

Forecast evaluation datasets

All forecasts will be evaluated against initial ECMWF Reanalysis version 5 (ERA5) release data (ERA5T).

For temperature and pressure

Forecasts will be evaluated against weekly averages computed from six-hourly data (0, 6, 12, and 18 UTC).

For precipitation

Forecasts will be evaluated against **weekly accumulations** derived from hourly data.

Forecast evaluation tools

To ensure **transparency and replicability** of the evaluation techniques used, participants can download the evaluation code and evaluate their forecasts using the AI-WQ-package Python package:

- `retrieve_evaluation_data.py` retrieves the required datasets including observations and climatological quintile boundaries.
- `forecast_evaluation.py` computes evaluation metrics.

The evaluation code should enable participants to **self-assess their forecasts** without competitive pressure during the Testing JJA period, which begins on **15 May 2025**.

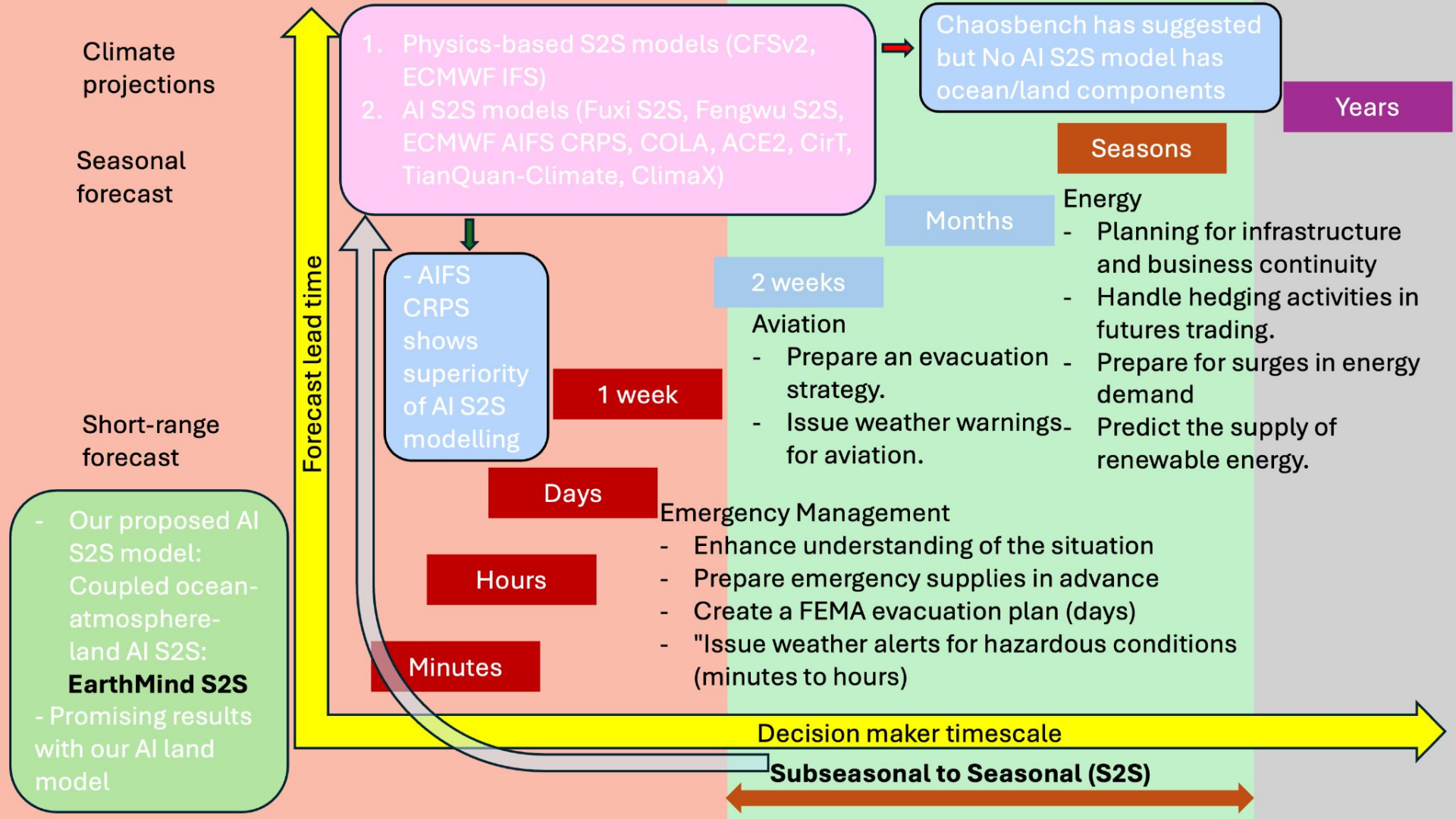
Climate projections
Seasonal forecast
Short-range forecast
Forecast lead time
1. Physics-based S2S models (CFSv2, ECMWF IFS)
2. AI S2S models (Fuxi S2S, Fengwu S2S, ECMWF AIFS CRPS, COLA, ACE2, CirT, TianQuan-Climate, ClimaX)
Chaosbench has suggested but No AI S2S model has ocean/land components
Years
Seasons
Months
2 weeks
1 week
Days
Hours
Minutes
- AIFS CRPS shows superiority of AI S2S modelling
Energy
- Planning for infrastructure and business continuity
- Handle hedging activities in futures trading.
- Prepare for surges in energy demand
- Predict the supply of renewable energy.
Aviation
- Prepare an evacuation strategy.
- Issue weather warnings for aviation.
Emergency Management
- Enhance understanding of the situation
- Prepare emergency supplies in advance
- Create a FEMA evacuation plan (days)
- "Issue weather alerts for hazardous conditions (minutes to hours)
- Our proposed AI S2S model: Coupled ocean-atmosphere-land AI S2S: EarthMind S2S
- Promising results with our AI land model
Decision maker timescale
Subseasonal to Seasonal (S2S)

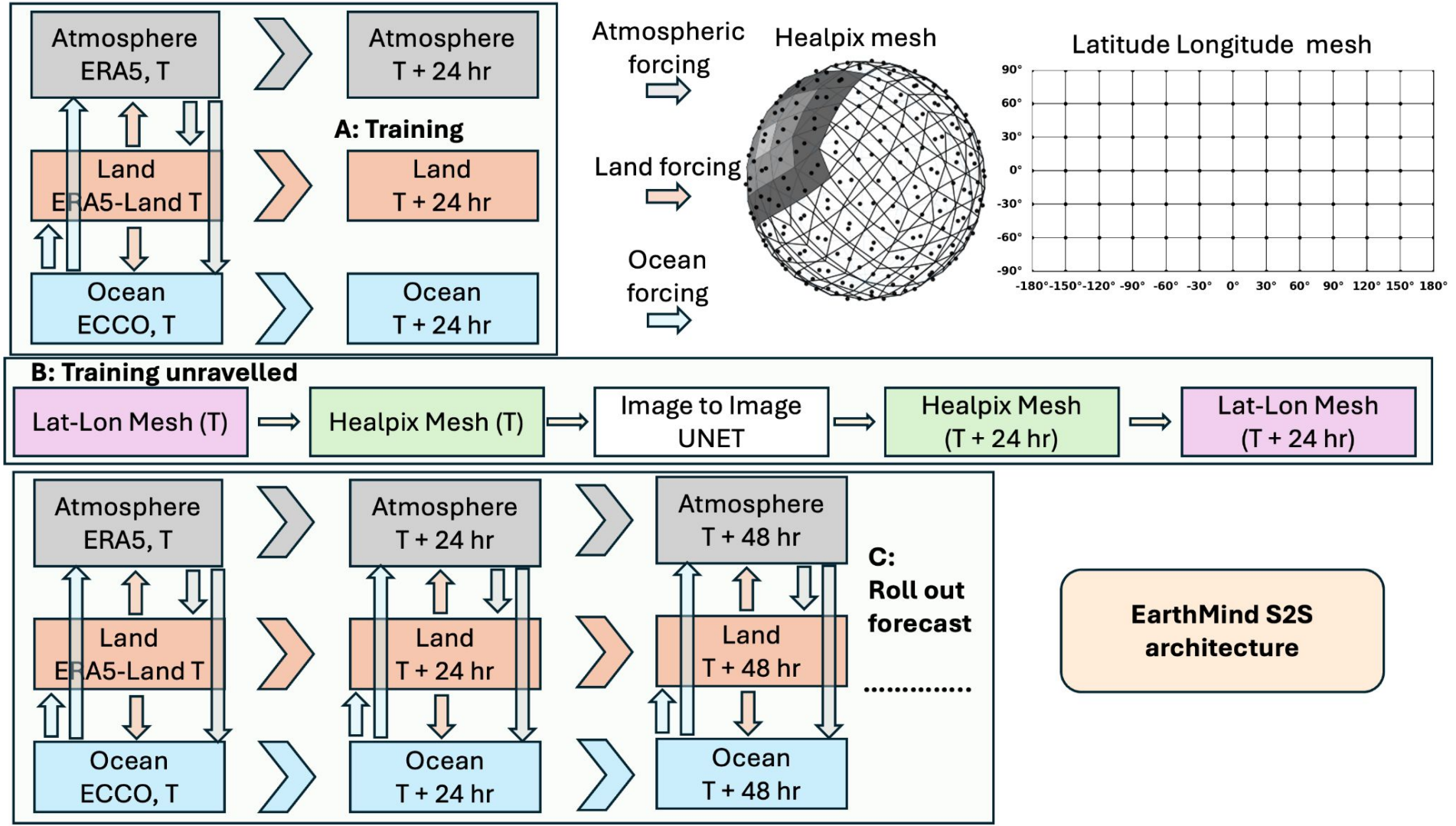
Atmosphere
ERA5, T
Atmosphere
T + 24 hr
A: Training
Land
ERA5-Land T
Land
T + 24 hr
Ocean
ECCO, T
Ocean
T + 24 hr
Atmospheric
forcing
Land forcing
Ocean
forcing
Healpix mesh
Latitude Longitude mesh
90°
60°
30°
0°
-30°
-60°
-90°
-180° -150° -120° -90° -60° -30° 0° 30° 60° 90° 120° 150° 180°
B: Training unravelled
Lat-Lon Mesh (T)
Healpix Mesh (T)
Image to Image
UNET
Healpix Mesh
(T + 24 hr)
Lat-Lon Mesh
(T + 24 hr)
Atmosphere
ERA5, T
Atmosphere
T + 24 hr
Atmosphere
T + 48 hr
Land
ERA5-Land T
Land
T + 24 hr
Land
T + 48 hr
Ocean
ECCO, T
Ocean
T + 24 hr
Ocean
T + 48 hr
C:
Roll out
forecast
.....
EarthMind S2S
architecture

AI-Land (HEALPix-U-Net) Pipeline

A Data & Preprocessing

ERA5-Land via
ARCO-ERA5 (Zarr, cloud-native)
(no download)

→ Hourly → Daily aggregation
(daily mean)

Initial state at day t
(all 17 channels)

Min-max normalize
(per variable)
(in lat-lon grid)

B Grid: HEALPix Level 6

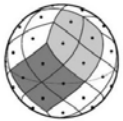

Lat-lon → HEALPix regridding (earth2grid)
Level = 6 (nside = 64) → 12 × 64 × 64 tiles
Tensor shape into model: [B, 17, 12, 64, 64]

C Model & Training

Input at day t:
X_t ∈ ℝ^{17×12×64×64}

→ 3D U-Net
3 encoder/decoder stages
• Conv3D(k=3), BN, ReLU
• Pool/Up: (1,2,2)
• Out: 8 channels

→ Targets at day t+1:
Y_{t+1} ∈ ℝ^{8×12×64×64}
(soil moisture & soil temp levels 1–4)

Training objective: learn f: X_t → Y_{t+1}
Loss: MSE Optimizer: Adam (lr=1e-3) Epochs per (t→t+1) pair: 10
Daily pairs from year; normalization stats fixed; tiles stay in HEALPix space

D Roll-out Forecasting

Day t input
(17 ch)

→ Predict day t+1
soil (8 ch)

Replace day t+1
soil in inputs

→ Predict day t+2
soil (8 ch)

Iterate for H steps to obtain multi-day roll-outs.
Optionally regrid outputs back to lat-lon and save (NetCDF).

E Input Variables & Normalization (min–max, lat-lon space)

Variable (min → max)	Variable (min → max)	Variable (min → max)
2m_temperature: 188 → 327	skin_temperature: 186 → 348	volumetric_soil_water_layer_4: -2.98e-08 → 0.766
total_precipitation: -3.73e-09 → 0.101	snowfall: -4.66e-10 → 0.0157	soil_temperature_level_1: 196 → 340
10m_u_component_of_wind: -281 → 133	mean_sea_level_pressure: 9e+04 → 1.1e+05	soil_temperature_level_2: 201 → 322
10m_v_component_of_wind: -159 → 167	volumetric_soil_water_layer_1: -0.0314 → 0.79	soil_temperature_level_3: 198 → 317
surface_solar_radiation_downwards: -6 → 4.89e+06	volumetric_soil_water_layer_2: -0.0204 → 0.788	soil_temperature_level_4: 181 → 315
evaporation: -0.00283 → 0.000733	volumetric_soil_water_layer_3: -0.0227 → 0.784	

All inputs normalized in lat-lon using fixed min/max, then regridded to HEALPix L6. Model predicts next-day soil variables; predictions are fed back for roll-outs.

AI-Land (HEALPix-U-Net) Pipeline

A Data & Preprocessing

ERAS-Land via
ARCO-ERAS (Zar, cloud-native)
(no download)

→ Hourly → Daily aggregation
(daily mean)

Initial state at day t
(17 channels)

Min-max normalize
(per variable
(in lat-lon grid)

B Grid: HEALPix Level 6

Lat-lon → HEALPix regridding
(convert 2D to 3D)
Level = 6 (nside 64) → 122 x 64 x 64 tiles
"Tensor" shape in model: [B, 17, 12, 64, 64]

C Model & Training

Input at day t
X_t ∈ R^(17×12×64×64)

3D U-Net
Encoder-Decoder stages
Conv(3×3)(B), BN, ReLU
• Pool/Up: (1,2,2)
• Out: 8 channels

Targets at day t+1
Y t+1, ∈ R^(8×164×64)
Soil moisture & soil temp levels 1-4,

Training objective: Learn f(X_t) → Y_(t+1)
Loss: MSE Optimizer: Adam (lr=1-3) Epochs per (t→t+1) pair: 10
Daily pairs from year, normalization stats fixed, tiles in HEALPix space

D Roll-out Forecasting

Day t input
(17 ch)

→ Predict day t+1
Soil (8 ch)

Replace day t+1
soil in inputs

→ Predict day t+2
Soil (8 ch)

Iterate for H steps to obtain multi-day roll-outs.
Optionally regrid outputs back to lat-lon and save (NetCDF)

E Input Variables & Normalization (min-max, lat-lon space)

Variable (min → max)
2m_temperature: 16.7 – 32.7
total_precipitation: 3.8e-09 – 0.101
10m_component_of_wind: -241 – 13.3
10m_component_of_wind: -19.9 – 16.7
surface_solar_radiation_downwards: 6 – 4.89e-06
evaporation: -0.00283 – 0.000733

Variable (min → max)
skin_temperature: 168 – 348
snowfall: -4.66e-06 – 0.501
mean_sea_level_pressure: 98014 – 1.1e-05
volumetric_soil_water_layer_1: 0.0316 – 0.79
volumetric_soil_water_layer_2: -0.0204 – 0.786
volumetric_soil_water_layer_3: -0.0227 – 0.784

Variable (min → max)
volumetric_soil_water_layer_4: -2.98e-08 – 0.766
soil_temperature_level_1: 196 – 340
soil_temperature_level_2: 130 – 204
soil_temperature_level_3: 198 – 317
soil_temperature_level_4: 181 – 315

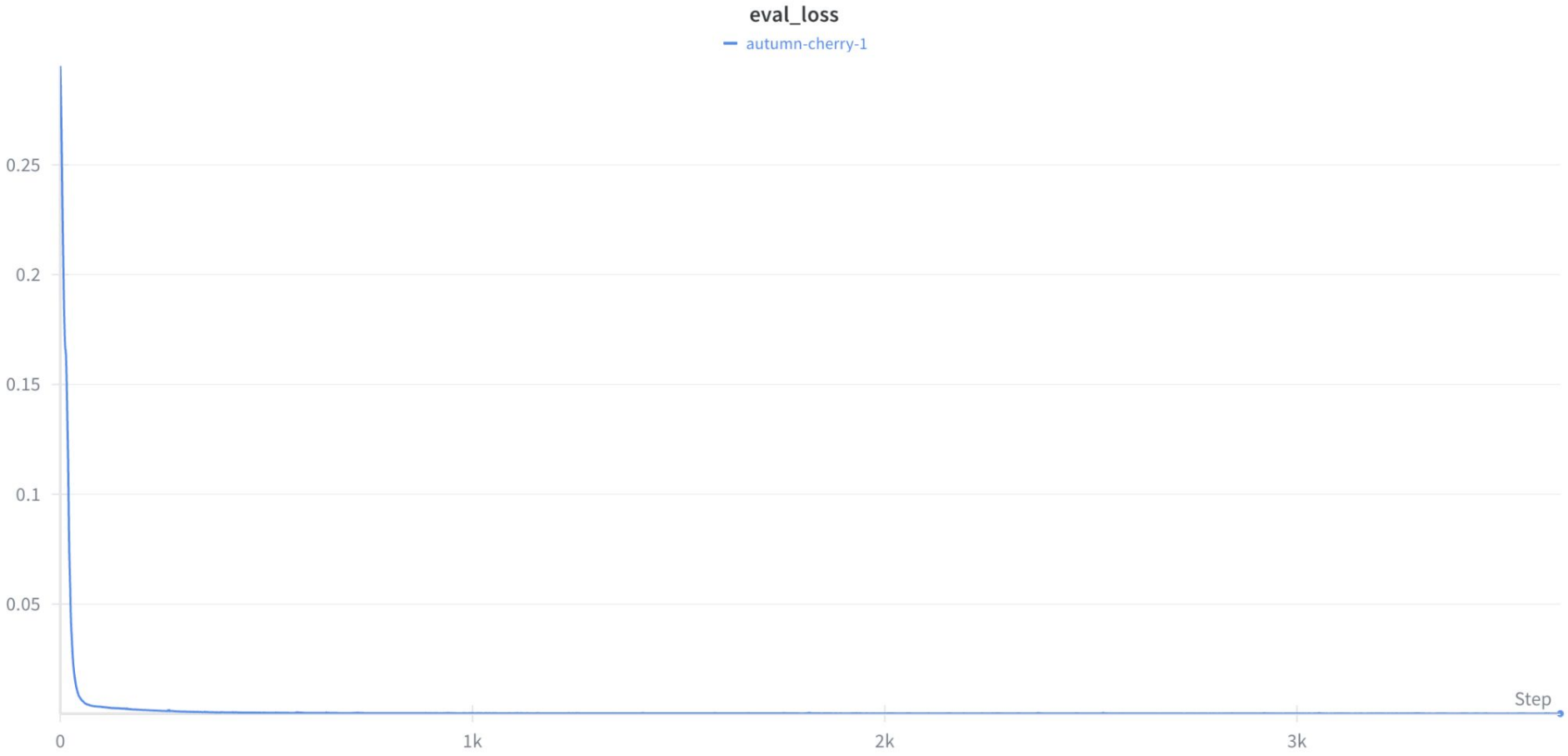
eval_loss
autumn-cherry-1
0.25
0.2
0.15
0.1
0.05
Step
0
1k
2k
3k

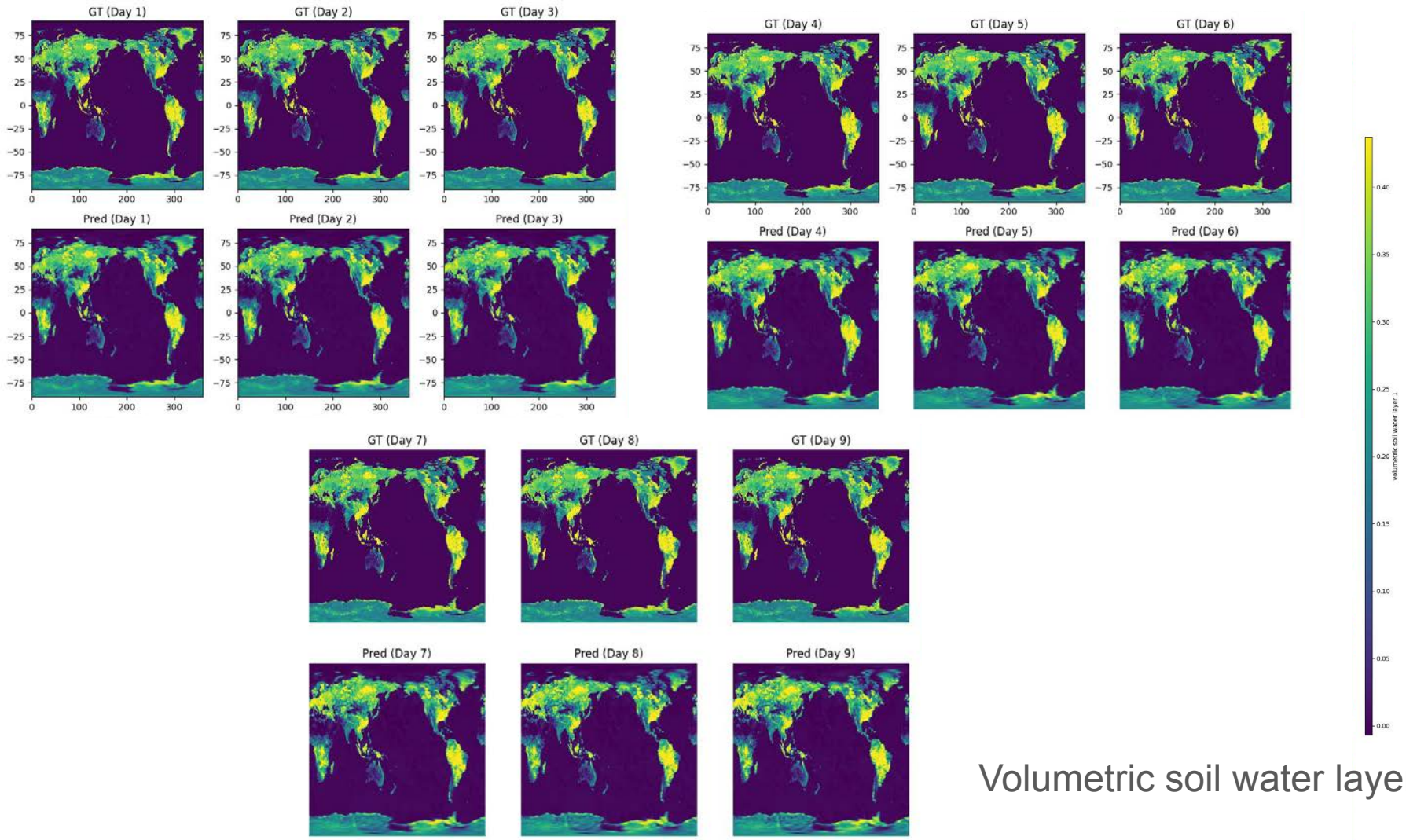

Volumetric soil water layer 1

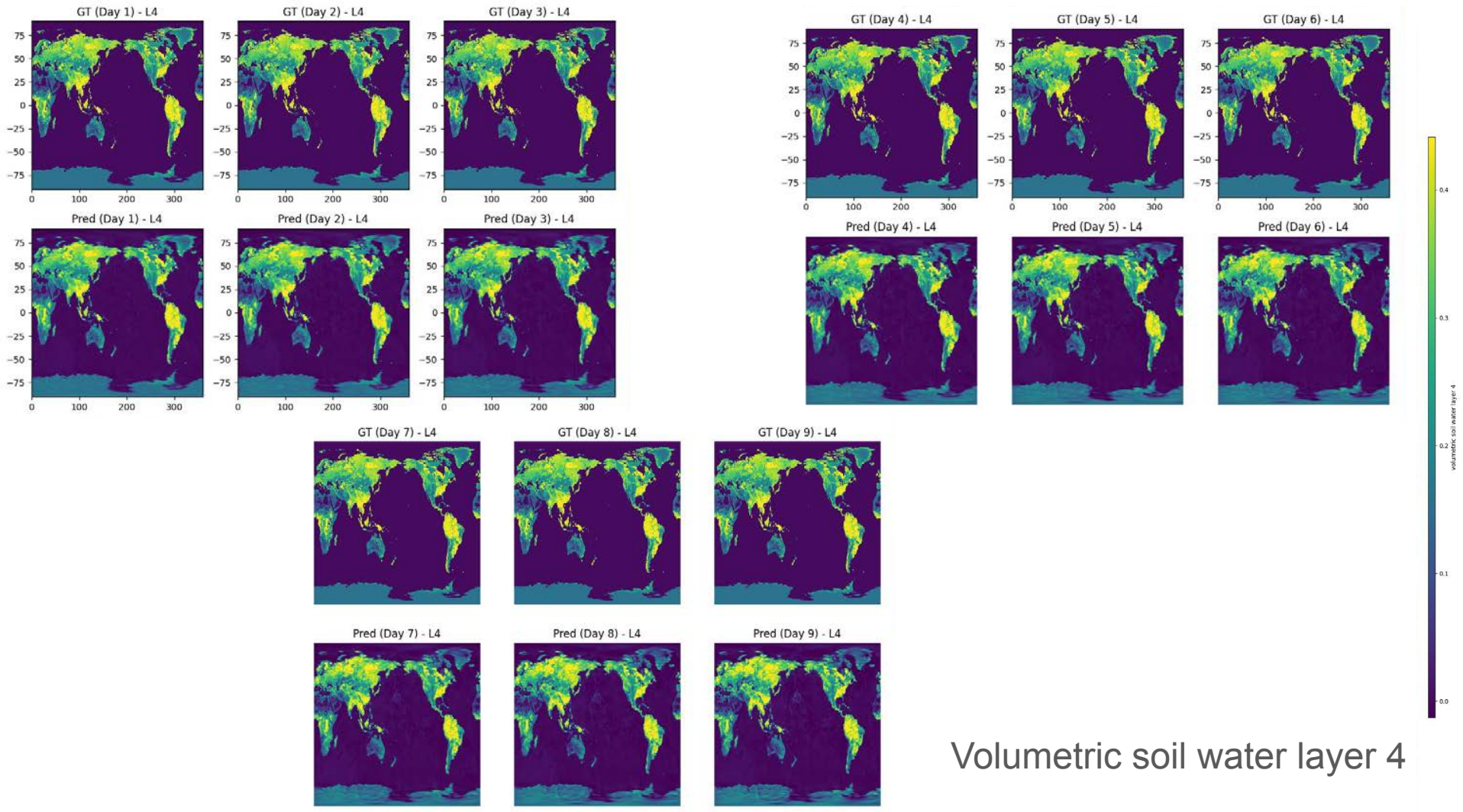

Volumetric soil water layer 4

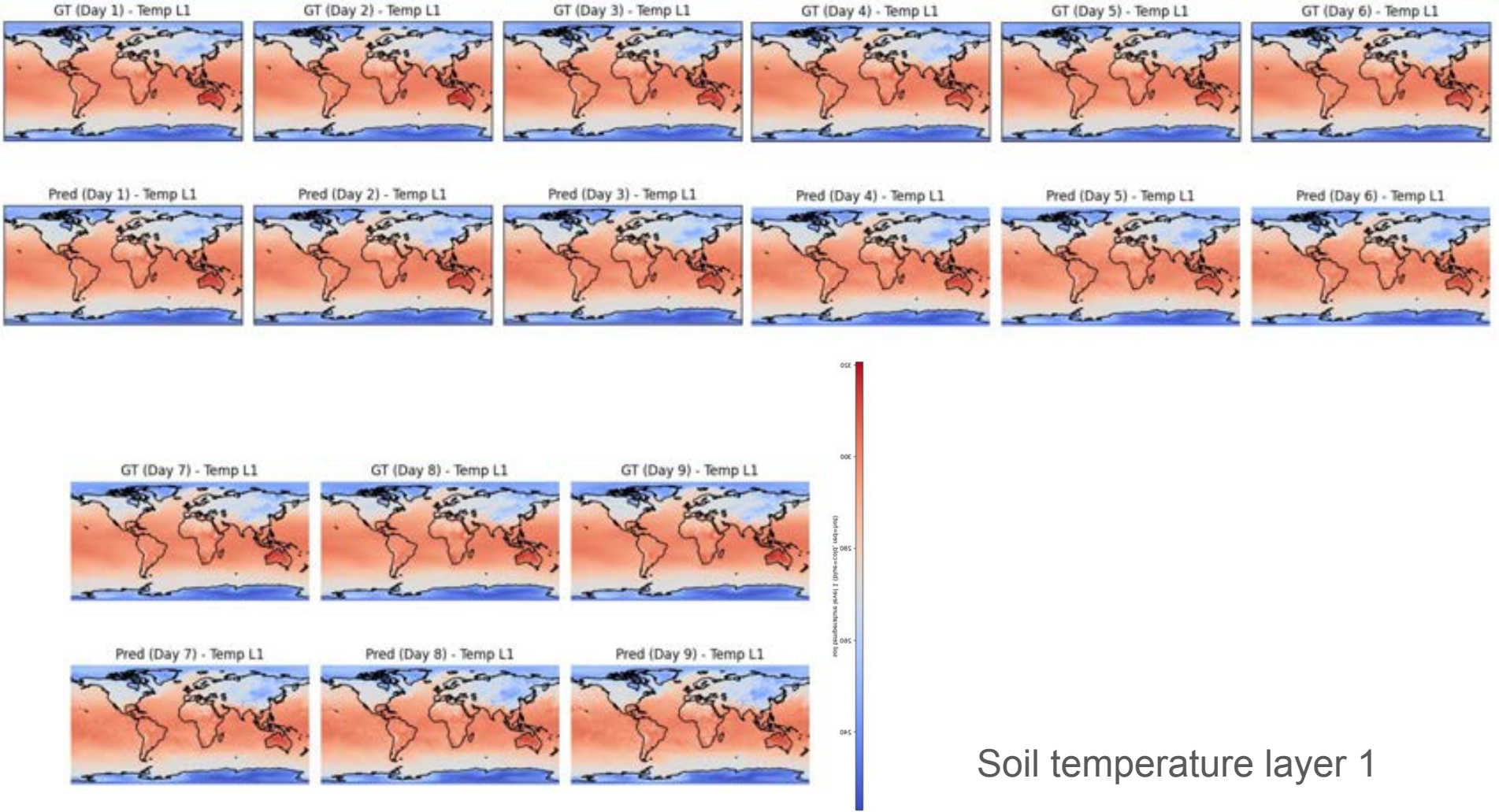

Soil temperature layer 1

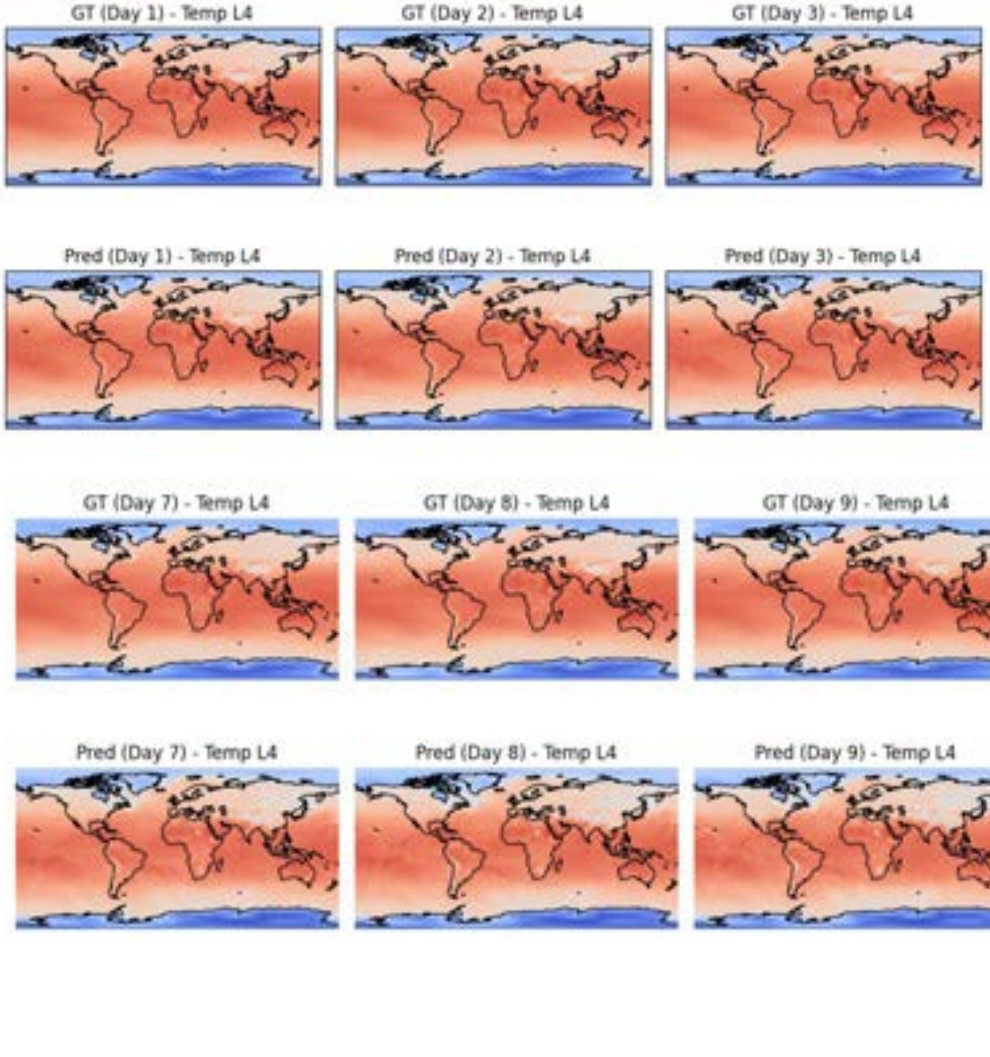

Soil temperature layer 4

Wet land event: 2019 Midwest / Mississippi Basin flooding 2019031500 IC

# US box (CONUS-ish)
lat_slice = slice(50, 25)
lon_slice = slice(-125, -65)

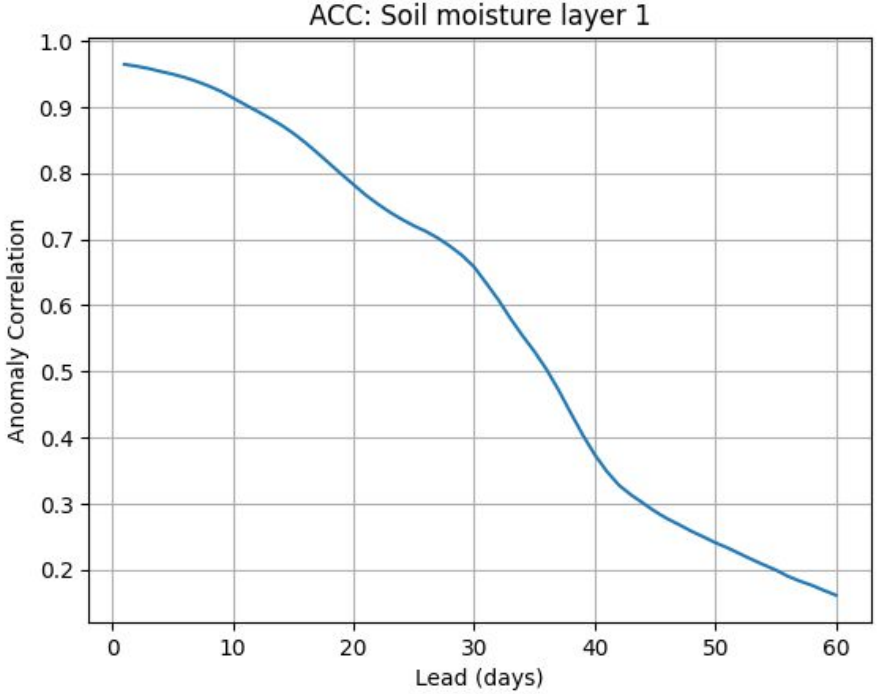

Flooding in the Mississippi River Basin during the winter, spring, and summer of 2019 caused at least 12 deaths and economic losses in 19 states totaling in excess of $20 billion. Estimated damages in the Midwestern United States alone had reached $12.5 billion by April 2019.

Wikipedia
https://en.wikipedia.org › wiki › Mississippi_River_floo...

Mississippi River floods of 2019 - Wikipedia

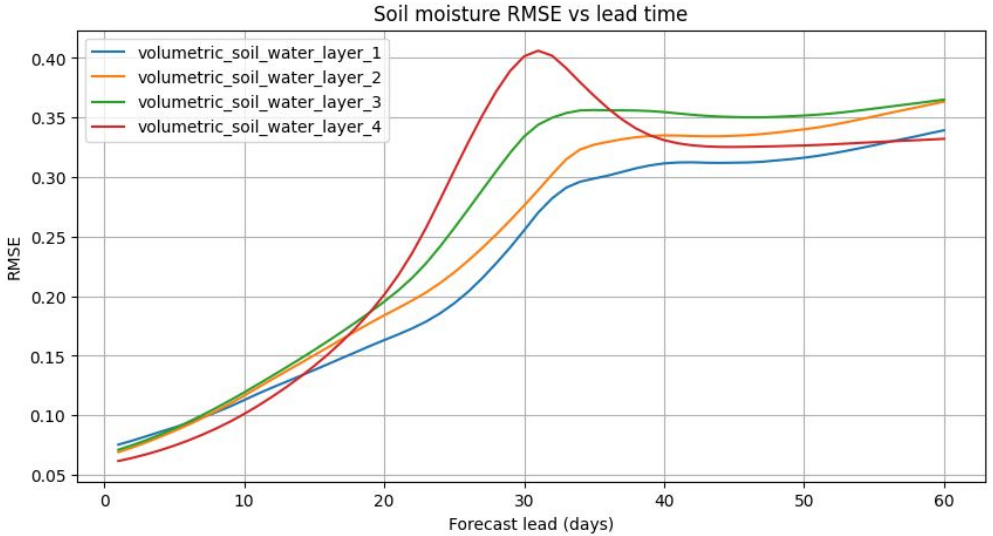

2012 Central US drought 2012051500 IC

The 2012 Central US drought, one of the worst on record, caused massive losses, with estimates ranging from **$30 billion to over $35 billion in agricultural damage alone**, impacting corn and soybean yields significantly and raising food prices. The overall economic impact on the U.S. GDP was potentially 0.5-1%, or $75-$150 billion, making it one of the costliest U.S. weather disasters, with lingering effects on livestock feed and food costs.

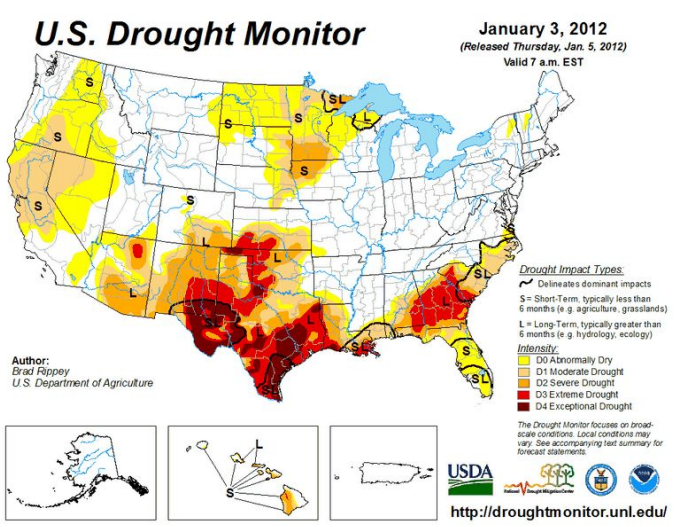

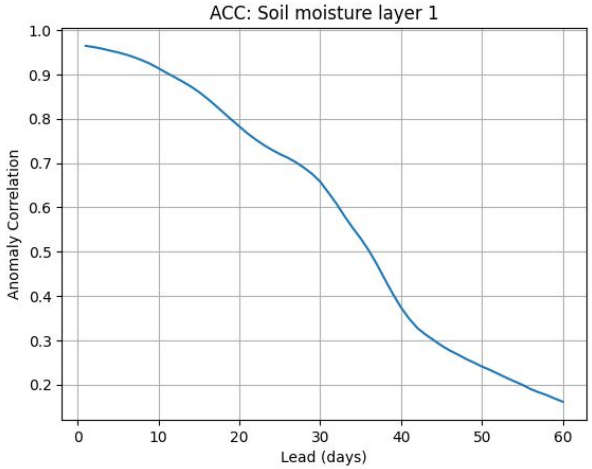

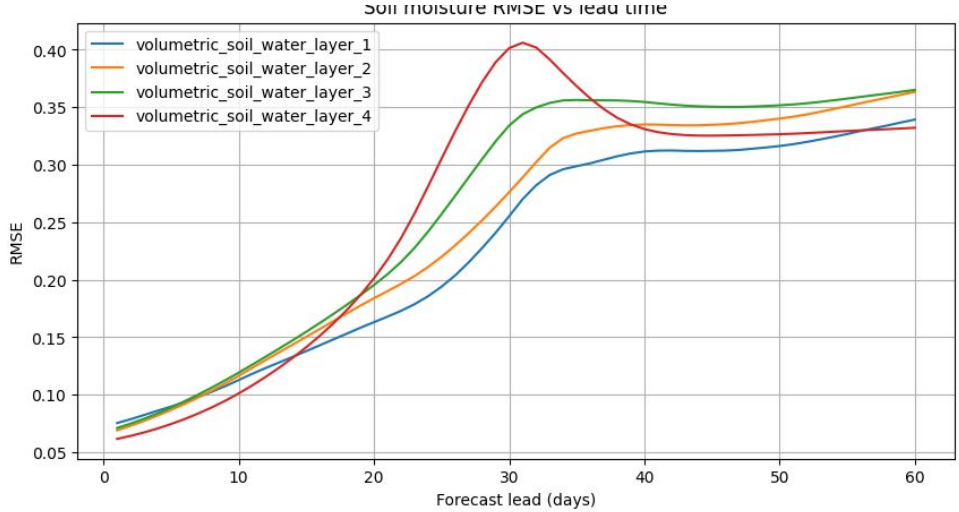

AI Ocean Model

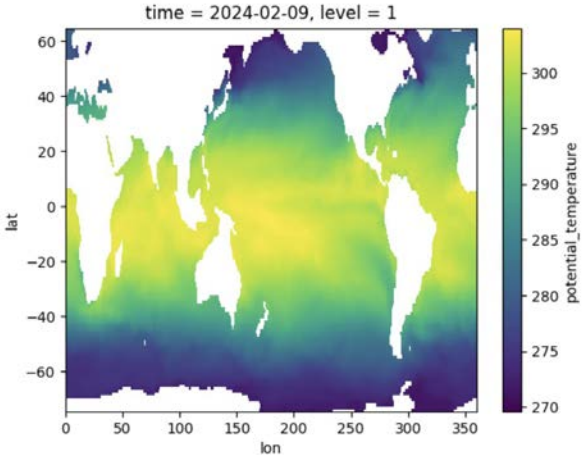

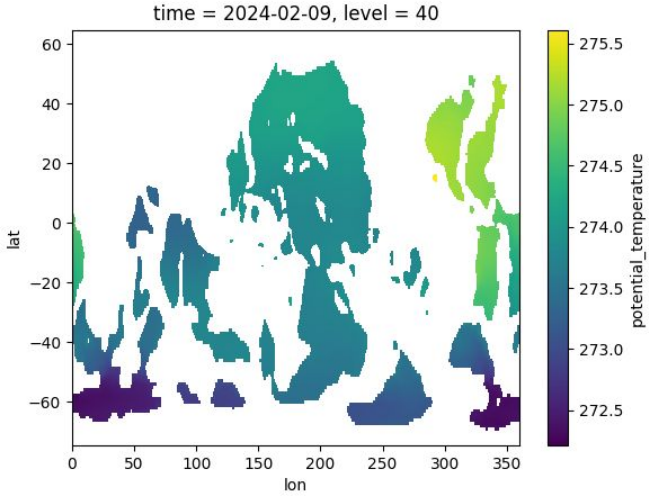

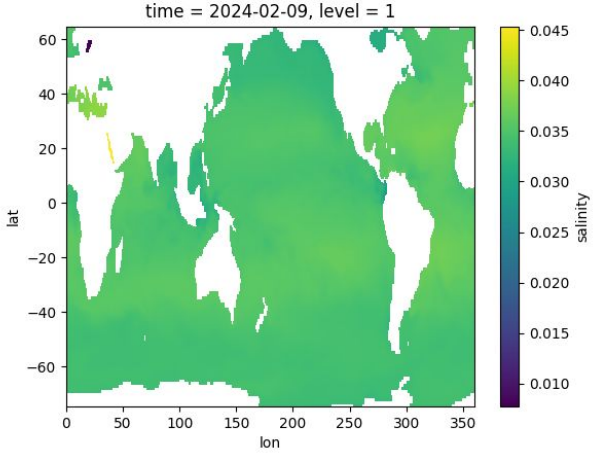

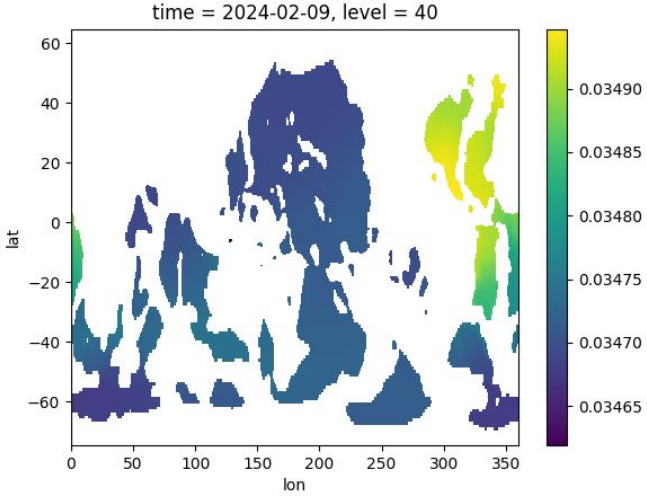

[u10, v10, sw_down, lw_down, t2m, q2m, precip, sp] - Atmospheric forcings from ERA5

Add a sparse tail below 300 m, e.g. [459, 747, 1193, 1807] m, to capture deeper thermocline/intermediate waters—still keeping the upper-ocean dense.

Levels that we will use : : [5, 15, 25, 45, 95, 155, 205, 303] m.

Indices these correspond to: 0, 1, 2, 4, 9, 15, 20, 25

Example of GODAS Pentad Timestamps

Pentad	Days Covered	Timestamp Shown in GODAS
Pentad 1	Jan 1–5	Jan 5
Pentad 2	Jan 6–10	Jan 10
Pentad 3	Jan 11–15	Jan 15
Pentad 4	Jan 16–20	Jan 20

Generative Data Assimilation of Sparse Weather Station Observations at Kilometer Scales

Peter Manshausen[1,2], Yair Cohen[1], Peter Harrington[1], Jaideep Pathak[1], Mike Pritchard[1,3], Piyush Garg[1], Morteza Mardani[1], Karthik Kashinath[1], Simon Byrne[1], Noah Brenowitz[1]

[1]NVIDIA, Santa Clara, CA, USA
[2]University of Oxford, Oxford, UK
[3]University of California Irvine, Irvine, CA, USA

Key Points:

- We demonstrate data assimilation of weather station data to 3km-resolution surface fields with a diffusion model surrogate.
- This opens up a simple, scalable pipeline to create km-scale ensemble reanalyses at low cost and latency, competitive to operational ones.
- The model is easily adapted to new observations, produces states of variables not directly observed, and shows evidence of learned physics.

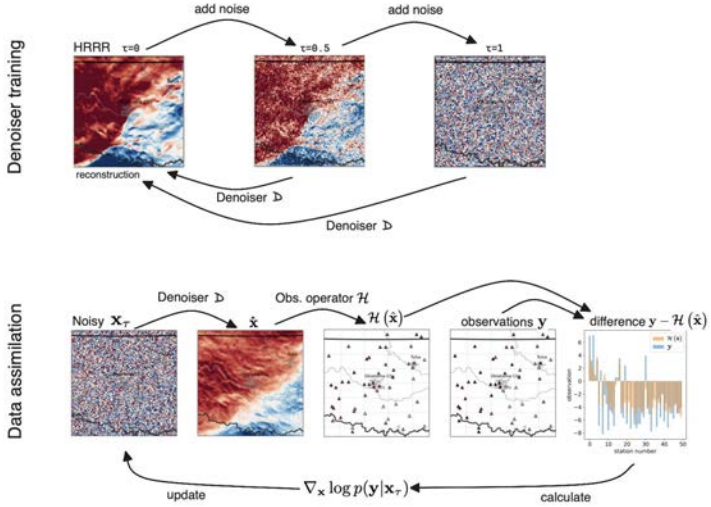

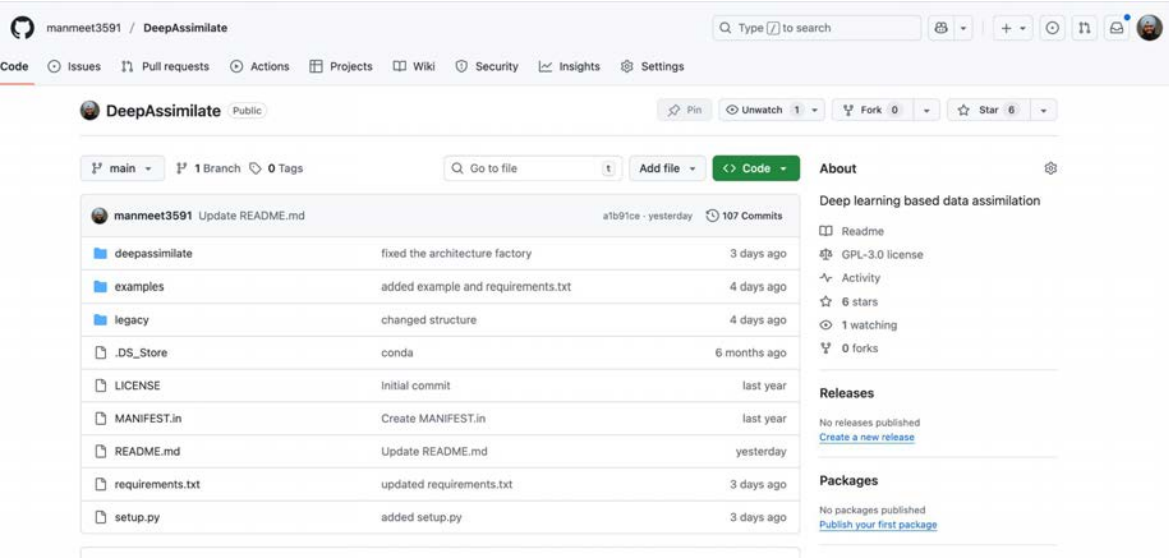

Precision Agriculture scale soil moisture data

A Concept

1. A generative diffusion model learns SMAP-HydroBlocks–like soil-moisture
2. Zero-shot data assimilation using diffusion produces 30 m, 6-hourly soil moisture.

B Training data & coverage

Target (train): SMAP-HydroBlocks, Kentucky, 30 m, Δt=6 h, 2015–2019
Coarse products: SMAP L4, 9 km, Δt=6 h (2015–2019)
Static predictors: soil properties, elevation

SMAP

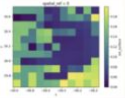

SMAP-HB

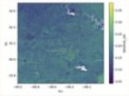

C Pipeline

Cube extraction (30 m, 64×64×T, e.g., T=4 steps) -> Normalize/mask -> Unconditional diffusion training $p_\theta(X)$ (3D denoiser on x–y–t) -> Inference init (noise cube) -> Apply forward ops H over time (e.g., per-step 9 km →30 m) -> Guided denoising with $\nabla_x \log p(Y|H(X))$ across the cube (zero-shot DA) -> Sample N ensemble cubes -> Stitch cubes in space/time -> Ensemble mean/spread, PI coverage -> Metrics vs SMAP-HB & stations -> 30 m, 6-hourly outputs.

F Kentucky Mesonet Validation

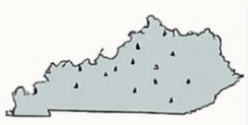

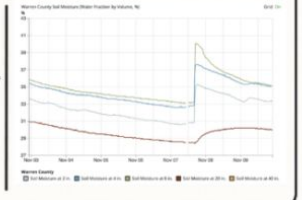

E Performance / Robustness

Power Spectral Density (PSD): compare texture/scale fidelity for *Held-out SMAP-HB (GT)* vs *Prior (unguided)* vs *Guided (zero-shot DA)*.
Accuracy metrics: R^2 (higher better), **ubRMSE** (lower), **Bias** (closer to 0).

G Uncertainty & ensembles

Montage	**Sharpness**
Mean/Spread	**Rank histogram**
Reliability	**CRPS**

H Generalization and OOD

OOD–Region: a different Kentucky Mesonet county
OOD–Time: a later year (e.g., 2020) over WKU Farm
OOD–Sensor: new sensors on WKU Farm

Diffusion and its derivatives everywhere

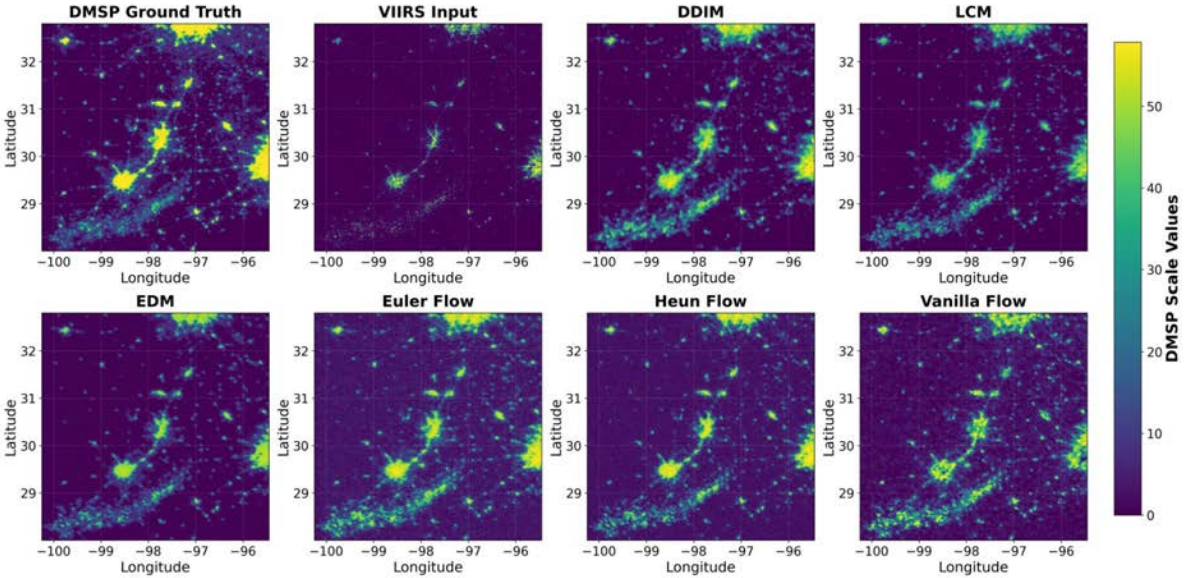

Method	SSIM	PSNR	MAE	MSE	RMSE	Inference Time
DDIM	0.6158	21.9123	0.0438	0.0064	0.0802	156.79s
LCM	0.6491	20.6988	0.0506	0.0085	0.0923	16.36s
EDM	0.5141	20.2804	0.0539	0.0094	0.0968	315.84s
Euler Flow	0.2247	19.7997	0.0757	0.0105	0.1023	154.56s
Heun Flow	0.2233	20.3246	0.0681	0.0093	0.0963	154.95s
Vanilla Flow	0.3637	20.6182	0.0581	0.0087	0.0931	134.91s
VIIRS	0.4137	12.5146	0.1110	0.05603	0.2367	-

Thank you